

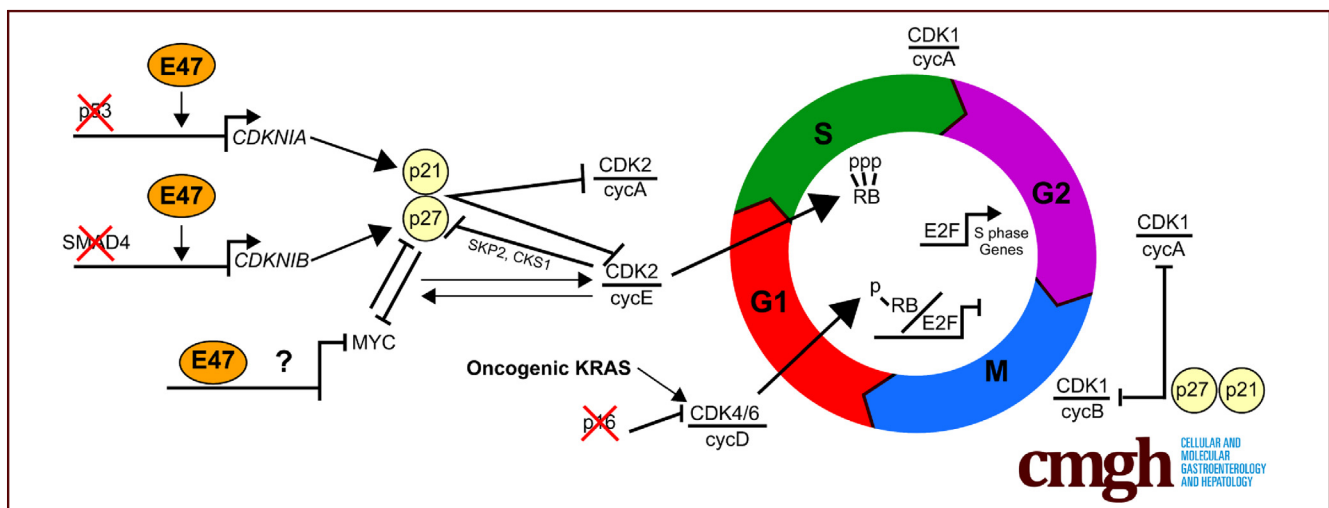
ORIGINAL RESEARCH

E47 Governs the MYC-CDKN1B/p27<sup>KIP1</sup>-RB Network to Growth Arrest PDA Cells Independent of CDKN2A/p16<sup>INK4A</sup> and Wild-Type p53



Kathleen M. Scully,<sup>1,\*</sup> Reyhaneh Lahmy,<sup>1,\*</sup> Lia Signaevskaia,<sup>1</sup> Roman Sasik,<sup>2</sup> Rachel Medal,<sup>1</sup> Heejung Kim,<sup>1</sup> Randall French,<sup>3</sup> Brian James,<sup>4</sup> Yifan Wu,<sup>1</sup> Andrew M. Lowy,<sup>3</sup> and Pamela Itkin-Ansari<sup>1,5</sup>

<sup>1</sup>Development, Aging and Regeneration Program, <sup>4</sup>Genomics Core, Sanford Burnham Prebys Medical Discovery Institute, La Jolla, California; <sup>2</sup>Center for Computational Biology and Bioinformatics, School of Medicine, <sup>3</sup>Department of Surgery, Division of Surgical Oncology, Moores Cancer Center, <sup>5</sup>Department of Pediatrics, University of California San Diego, La Jolla, California



SUMMARY

The basic helix-loop-helix transcription factor E47 arrests proliferation and elicits cellular senescence in pancreatic ductal adenocarcinoma cell lines. The molecular mechanisms involve alterations in both RNA transcript levels and proteosomal degradation of MYC and CDKN1B/p27<sup>Kinase Inhibitory Protein 1</sup>, resulting in rearming of retinoblastoma tumor-suppressor function.

**BACKGROUND & AIMS:** Oncogenic mutations in KRAS, coupled with inactivation of p53, CDKN2A/p16<sup>INK4A</sup>, and SMAD4, drive progression of pancreatic ductal adenocarcinoma (PDA). Overexpression of MYC and deregulation of retinoblastoma (RB) further promote cell proliferation and make identifying a means to therapeutically alter cell-cycle control pathways in PDA a significant challenge. We previously showed that the basic helix-loop-helix transcription factor E47 induced stable growth arrest in PDA cells in vitro and in vivo. Here, we identified molecular mechanisms that underlie E47-induced growth arrest in low-passage, patient-derived primary and established PDA cell lines.

**METHODS:** RNA sequencing was used to profile E47-dependent transcriptomes in 5 PDA cell lines. Gene Ontology analysis identified cell-cycle control as the most altered pathway. Small interfering RNA/short hairpin RNA knockdown, small-molecule inhibitors, and viral expression were used to examine the function of E47-dependent genes in cell-cycle arrest. Cell morphology, expression of molecular markers, and senescence-associated  $\beta$ -galactosidase activity assays identified cellular senescence.

**RESULTS:** E47 uniformly inhibited PDA cell-cycle progression by decreasing expression of MYC, increasing the level of CDKN1B/p27<sup>KIP1</sup>, and restoring RB tumor-suppressor function. The molecular mechanisms by which E47 elicited these changes included altering both RNA transcript levels and protein stability of MYC and CDKN1B/p27<sup>KIP1</sup>. At the cellular level, E47 elicited a senescence-like phenotype characterized by increased senescence-associated  $\beta$ -galactosidase activity and altered expression of senescence markers.

**CONCLUSIONS:** E47 governs a highly conserved network of cell-cycle control genes, including MYC, CDKN1B/p27<sup>KIP1</sup>, and RB, which can induce a senescence-like program in PDA cells that lack CDKN2A/p16<sup>INK4A</sup> and wild-type p53. RNA

sequencing data are available at the National Center for Biotechnology Information GEO at <https://www.ncbi.nlm.nih.gov/geo/>; accession number: GSE100327. (*Cell Mol Gastroenterol Hepatol* 2018;6:181–198; <https://doi.org/10.1016/j.jcmgh.2018.05.002>)

**Keywords:** Pancreatic Ductal Adenocarcinoma; bHLH; Cell Cycle; Senescence.

See editorial on page 223.

**D**evelopment of pancreatic ductal adenocarcinoma (PDA) is a slow process that most often begins with acquisition of an oncogenic KRAS mutation in cells of the exocrine pancreas.<sup>1–5</sup> In response to constitutively active KRAS, cells can enter oncogene-induced senescence (OIS), a state of cell-cycle arrest that generally is established and maintained by p53 and its target gene, CDKN1A/p21<sup>CIP1</sup>, in combination with CDKN2A/p16<sup>INK4A</sup>-mediated activation of the retinoblastoma (RB) tumor-suppressor pathway.<sup>6,7</sup> Additional extracellular signals such as pancreatitis-associated inflammation, however, subvert OIS and initiate acinar-to-ductal metaplasia.<sup>8</sup> Subsequent silencing, mutation, or loss of the tumor-suppressor genes p53, CDKN2A/p16<sup>INK4A</sup>, and SMAD4 promote further disease progression.<sup>9</sup>

Although RB is rarely mutated or silenced in PDA, the frequent loss of its critical upstream regulator, CDKN2A/p16<sup>INK4A</sup>, results in cyclin-dependent kinase (CDK)-mediated phosphorylation of RB, which disables RB tumor-suppressor function.<sup>10</sup> Similarly, although the CDKN1A/p21<sup>CIP1</sup> gene itself is not usually altered in PDA, its upstream regulator, p53, often harbors DNA binding domain mutations that disrupt its ability to activate CDKN1A/p21<sup>CIP1</sup> transcription.<sup>10,11</sup> In PDA, as in many other cancers, amplification and increased expression of the MYC locus are common and correlated with poor prognosis.<sup>10,12</sup> Moreover, MYC is sufficient to initiate and drive progression of pancreatic tumors in vivo whereas MYC knockdown promotes a latent program of cellular senescence.<sup>13,14</sup>

Early in acinar-to-ductal metaplasia, acinar cells gain proliferative potential and lose characteristics of their differentiated phenotype. These changes are associated with decreased expression of the tissue-specific basic helix-loop-helix (bHLH) transcription factors PTF1A and MIST1, which function through heterodimerization with ubiquitously expressed bHLH E proteins (E47, E12, HEB, and E2-2). The joint basic domains of the heterodimers form a single DNA binding motif that recognizes the sequence CANNTG in target genes that promote and maintain the differentiated acinar cell phenotype.<sup>3,15,16</sup> Loss of bHLH proteins is exacerbated by concurrent increased expression of ID1–3 (Inhibitor of DNA binding 1–3). IDs are HLH proteins that lack a basic domain and form non-DNA binding dimers preferentially with bHLH E proteins. The ID4 locus, in contrast, has been reported to be hypermethylated and hence silenced in pancreas cancer.<sup>17</sup> We and others have observed increased expression of ID1–3 proteins in response to chronic pancreatitis and in PDA.<sup>18–20</sup> Moreover, we have

shown that overexpression of ID3 alone, in normally quiescent primary human pancreatic exocrine cells, is sufficient to trigger cell-cycle entry.<sup>19</sup> Thus, the ratio of ID to bHLH proteins may determine the balance between differentiation and proliferation in the exocrine pancreas.

In addition to promoting differentiation through heterodimerization with tissue-specific bHLHs, E protein homodimers can direct a concerted transcriptional program that controls cell-cycle progression.<sup>21</sup> In the established PDA cell lines BxPC-3, MIA PaCa-2, and PANC-1, we previously showed that E47 blocked proliferation, in part, through up-regulation of CDKN1A/p21<sup>CIP1</sup>. To identify additional molecular mechanisms and enhance clinical relevance, we used 2 new low-passage number, patient-derived cell lines: 1 from a primary PDA tumor and the other from a PDA liver metastasis in a different patient. Here, we report that E47 uniformly blocked the growth of these genetically diverse pancreas cancer cell lines by systematically altering the expression of a large cohort of genes involved in cell-cycle regulation. Mechanistically, E47 blocked cell proliferation by decreasing MYC expression, up-regulating CDKN1B/p27<sup>KIP1</sup> levels, and rearming RB to function as a tumor suppressor. At the cellular level, E47 induced a senescence-like phenotype.

## Materials and Methods

### Cell Culture

ATCC (Rockville, MD) cell line culture was as previously described.<sup>22</sup> Cell lines 1334 and 779e were grown in high-glucose Dulbecco's modified Eagle medium, initially supplemented with 30% fetal bovine serum, 2 mmol/L glutamine, 1 mmol/L sodium pyruvate, 1× nonessential amino acids, 200 IU/mL penicillin, 0.2 mg/mL streptomycin, and 1× Fungizone (Thermo Fisher Scientific, San Diego, CA). All cells were grown in 5% CO<sub>2</sub> at 37°C.

### Generation of E47-Expressing Cell Lines

The generation of E47-expressing cell lines was as previously described.<sup>22</sup> Nuclear E47 was induced with 4 μM 4-hydroxytamoxifen for 48–72 hours unless otherwise noted.

\*Authors share co-first authorship.

**Abbreviations used in this paper:** bHLH, basic helix-loop-helix; CDK, cyclin-dependent kinase; CDKN1B/p27<sup>KIP1</sup>, CDKN1B/p27<sup>Kinase Inhibitory Protein 1</sup>; CDKN2A/p16<sup>INK4A</sup>, CDKN2A/p16<sup>Inhibitor of CDK 4A</sup>; CEBP-α, CCAAT/enhancer binding protein alpha; CENP-A, centromere protein A; CIP, Cyclin-Dependent Kinase Inhibitor 1; DDR, DNA damage response; ERK, extracellular signal-regulated kinase; GO, Gene Ontology; lfr, local false discovery rate; INK, Inhibitor of CDK; KIP, Kinase Inhibitory Protein; mRNA, messenger RNA; MSCV, murine stem cell virus; OIS, oncogene-induced senescence; PCR, polymerase chain reaction; PDA, pancreatic ductal adenocarcinoma; RB, retinoblastoma; RNA-seq, RNA sequencing; SA-βgal, senescence-associated β-galactosidase; shRB, short hairpin RNA directed against RB; shRNA, short hairpin RNA; si-p27, small interfering RNA directed against p27; SKP, S-phase Kinase-associated.

Most current article

© 2018 The Authors. Published by Elsevier Inc. on behalf of the AGA Institute. This is an open access article under the CC BY-NC-ND license (<http://creativecommons.org/licenses/by-nc-nd/4.0/>).

2352-345X

<https://doi.org/10.1016/j.jcmgh.2018.05.002>

### Exome Sequencing

Genomic DNA extracted from 1334 and 779e cells was subjected to whole-exome sequencing (SBP Medical Discovery Institute Genomics Core, La Jolla, CA). Libraries, made using the Ion AmpliSeq Exome Kit, were sequenced on an Ion Proton with 2 barcoded libraries loaded per PI chip (Life Technologies, Carlsbad, CA). At least 35 million reads per sample were generated. Reads were aligned to the human genome hg19 version in Torrent Suite v4.2. Variants were called with Torrent Suite Variant Caller v4.2 and annotated with ANNOVAR (<http://www.openbioinformatics.org/annovar/>).

### Confirmation of Exome Sequencing

Regions of driver loci that contained mutations were polymerase chain reaction (PCR)-amplified and subjected to Sanger sequencing. Oligos used to amplify KRAS DNA were as follows: KRAS-F3 5'-GCCTGCTGAAAATGACTGAATA TAAAC-3' and KRAS-R1 5'-GGACTGGGGAGGGCTTTCTTTG-3'. Oligos used to amplify p53 exon 5 DNA IN 1334 cells were as follows: hup53exon5-F1 5'-TACTCCCCTGCCCT CAACAAG -3' and hup53exon5-R1 5'-ATCGCTATCTGAG CAGCGCTC-3'. Oligos used to amplify p53 exon 6 DNA in 779e cells were as follows: hup53exon6-F1 5'-GGTCTGGCCCTCCTCAGCAT-3' and hup53exon6-R1 5'-CTCAGGCGGCTCATAGGGCAC-3'.

### Cell Line Authentication

Short tandem repeat analysis was performed on genomic DNA from ATCC human pancreatic adenocarcinoma cell lines BxPC-3 (CRL-1687), MIAPaCa-2 (CRL-1420), and PANC-1 (CRL-1469) with GenePrint 10 System (Promega, Madison, WI). Peaks were analyzed using GeneMarker HID (Softgenetics, State College, PA). Allele calls were searched against short tandem repeat databases maintained by ATCC ([www.atcc.org](http://www.atcc.org)), Deutsche Sammlung von Mikroorganismen und Zellkulturen ([www.dsmz.de](http://www.dsmz.de)), and the Texas Tech University Children's Oncology Group ([cogcell.org](http://cogcell.org)).

### Flow Cytometry

Flow cytometry was as previously described.<sup>22</sup>

### Library Construction and RNA Sequencing

Total RNA was isolated from cells using an RNeasy Mini Kit (Qiagen, Frederick, MD). All samples had RNA integrity number scores of 8.3 or higher. Libraries were generated using TruSeq Stranded messenger RNA (mRNA) Sample Prep Kits (Illumina, San Diego, CA) following the manufacturer's instructions, with shear time modified to 5 minutes. RNA sequencing (RNA-seq) samples were run on Illumina HiSeq2500 and HiSeq4000 (Rapid Run and V4 chemistry).

### RNA-Seq Analysis

RNA-seq fastq files with approximately  $40 \times 10^6$  reads per sample were processed into transcript-level summaries using *kallisto* (<https://pachterlab.github.io/kallisto/about>). The reference transcriptome was current human GENCODE

(<https://www.encodegenes.org>) release 23 (GRCh38.p3). Transcript-level summaries were combined into gene-level summaries by adding all transcript counts from the same gene. Gene counts were normalized across samples using Differential Expression of RNA-seq normalization. The gene list was filtered based on the mean abundance (across samples), which left approximately 15,500 detected genes for further analysis. Differential expression was assessed with an R package *limma* applied to  $\log_2$ -transformed counts. The statistical significance of each test was expressed in terms of local false discovery rate (lfr) using the *limma* function Empirical Bayes Statistics for Differential Expression.

### Principal Component Analysis

The integrity of the experiment, based on the consistency of replicates and the direction of treatment effects, was assessed globally by principal component analysis using R.

### Statistical Analysis

To identify genes that responded similarly to E47 in all 5 cell lines, we defined a statistic,  $s$ , that combined statistical significance with magnitude of change into a single number for each cell line, where  $s = -\log_{10}(\text{lfr}) * \log_2(\text{with tamoxifen/no tamoxifen})$ . A second statistic,  $s_5$ , combined the magnitude of response of a given gene in individual cell lines with consistency across all cell lines examined. This was a 5-dimensional vector  $\vec{s}$ , whose first component was  $s$  measured in the first cell line, and so forth. Genes that responded to E47 equivalently in all cell lines had large and similar  $s$  coordinates. We then constructed a single scalar statistic as follows:  $s_5 = (\vec{s} \cdot \vec{n})^2 - [\vec{s} - (\vec{s} \cdot \vec{n})\vec{n}]^2$ , where  $\vec{s} \cdot \vec{n}$  denotes the scalar product and  $\vec{n} \equiv (1, 1, 1, 1, 1)/\sqrt{5}$  is the unit vector in the direction of the body diagonal. Genes were sorted by  $s_5$  in descending order.

### Conditional Gene Ontology Analysis

The Gene Ontology (GO) Biological Process category is a directed graph of terms, each of which may have several daughter and parent terms. Each term contains genes assigned to it either directly or via its daughter terms and their descendants. To reduce redundancy and dependencies between GO terms, we performed conditional GO analysis by levels, with each level conditional on the previous level. Terms enriched for genes from the  $s^5 > 100$  set emerged from all genes detected in the 5 cell lines. In level 1, we tested all GO terms without daughter terms (ie, the most specific terms farthest from the root of the GO graph). For each such term, hypergeometric raw  $P$  values were converted to posterior error probabilities using Storey's theory and *lfr* function in the R package *q* value. All terms with *lfr* < 0.01 were called significant at level 1 and their genes were marked as used. Next, we calculated the probability that a level 2 term would be at least as enriched by genes from the small set as observed given that some of the genes already had been used. Conditional  $P$  values were assigned using the same hypergeometric formula, but the number of genes was reduced by the

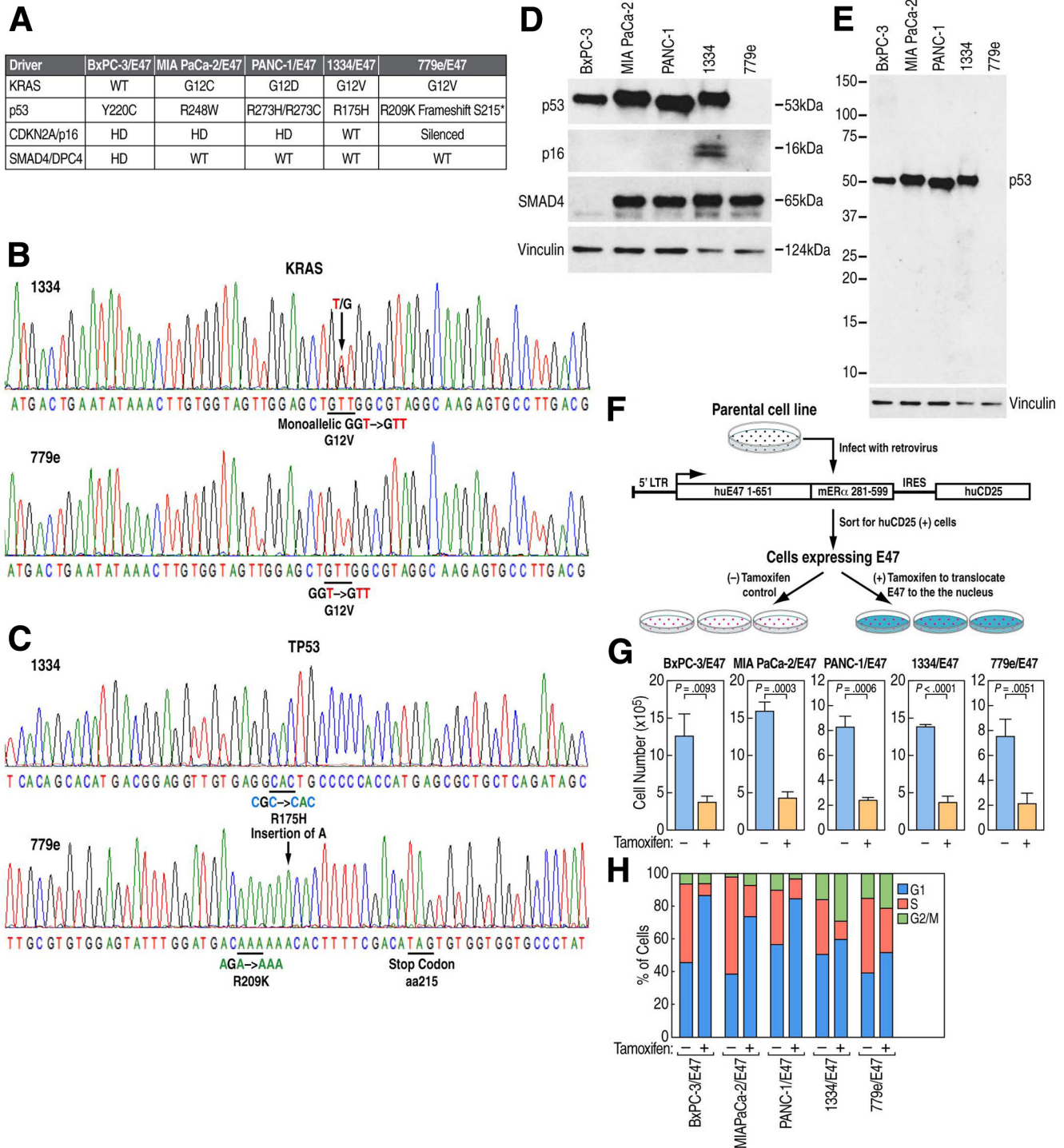


**Figure 1. E47 inhibits proliferation of 5 genetically diverse established and patient-derived primary PDA cell lines.** (A) Exome sequencing identified the genetic status of the 4 most common driver loci in 1334 and 779e primary lines. S215\* is a premature truncation. Information on BxPC-3, MIA PaCa-2, and PANC-1 cells.<sup>24</sup> (B) Sanger sequencing of PCR-amplified genomic DNA confirmed mutations initially identified by exome sequencing. The KRAS locus harbors a G12V mutation that appears mono-allelic in 1334 cells. (C) In 1334 cells, a missense mutation results in R175H at the p53 locus. In 779e cells, a missense mutation causes R209K and is followed by a single base insertion that produces N210K, T211H, F212F, R213S, H214T, and a premature stop S215\*. (D) Western blot of 25 µg of whole-cell extracts. (E) A longer exposure of full-length p53 blot. No p53 is detectable in 779e whole-cell extracts probed with mouse anti-p53 (Ab-6 clone DO-1, M-187-P0; Neomarkers, Fremont, CA). (F) Infection of PDA cell lines with a retrovirus encoding full-length human E47 fused to the murine estrogen receptor ligand binding domain modified to respond to tamoxifen followed by selection for human CD25 as previously described.<sup>22</sup> Selected cells were treated with 4 µM 4-hydroxytamoxifen for 48–72 hours to induce nuclear localization of the E47 fusion protein. (G) Equal numbers of cells were plated, treated to induce E47, and counted. Data represent the mean of 3 independent biological replicates analyzed by an unpaired *t* test. Error bars are ± SEM. (H) Percentages of cells in specific phases of the cell cycle were identified by flow cytometry as previously described.<sup>22</sup> HD, homozygous deletion; WT, wild-type.

number used. *P* values from level 2 were converted to posterior error probabilities and terms with *lfdr* < 0.01 were called conditionally significant at level 2. The process continued until the only remaining term was the root node: Biological Process. The entire table of significant terms was reported (Figure 2E).

### Cell-Cycle PCR Array Analysis

The expression of 84 cell-cycle-regulated genes was examined using a Human Cell Cycle RT<sup>2</sup> Profiler PCR array and software (Qiagen, SA Bioscience) according to the manufacturer's instructions. Briefly, total RNA was extracted from 3 independent samples of 1334/E47 and 779e/E47 cells ± tamoxifen treatment to induce nuclear localization of E47. Complementary DNA was prepared from 1 µg total RNA and subjected to PCR analysis (RT<sup>2</sup> Profiler PCR array data analysis software, v3.5).

### Pathway Analysis

The sorted list of genes was analyzed for over-represented biological processes and pathways using a nonparametric version of Gene Set Enrichment Analysis.

### Cell Size Determination

Cell size was measured using the ImageJ (National Institutes of Health, Bethesda, MD) freehand selection tool to outline cells after staining with 5 µg/mL wheat germ agglutinin conjugated to Alexa 488 (cat. W11261; Invitrogen/Molecular Probes, Eugene, OR).

### Senescence-Associated β-Galactosidase Assays

Activity was assayed at pH 6 after 72 hours of culture using a senescence β-Galactosidase Staining Kit (cat. no. 9860; Cell Signaling, Danvers, MA) following the manufacturer's instructions.

### Small Interfering RNA Directed Against p27 and Short Hairpin RNA Directed Against RB

Small interfering RNA directed against p27 (si-p27) ID J-003472-05 and J-003472-06 (Dharmacon, Lafayette, CO). Murine stem cell virus (MSCV)-short hairpin RNA directed against RB (shRB-1) and MSCV-ctrl retroviral vectors were a generous gift from Scott Lowe. shRB-1 target sequence 5'-GAAAGGACATGTGAACCTTA-3'. pSLIK shRB (shRB-2) 1534 hyg lentiviral vector was from Julien Sage (Addgene 31500), with target sequence 5'-GAACGATTATCCATCCAAA-3'.

### Viral Expression of Mouse Rb and Human MYC

Retroviral puromycin-resistant MSCV N-terminal hemagglutinin-tagged wild-type mouse Rb was a generous gift from Steve Dowdy (University of California, San Diego, CA). Lentiviral wild-type and T58A human MYC vectors were a generous gift from Yanxin Pei (Children's National Medical Center, Washington, DC).

### Antibodies Used

See Table 1.

## Results

### Genetic Status of PDA Driver Loci Determined in Primary Patient-Derived Cell Lines

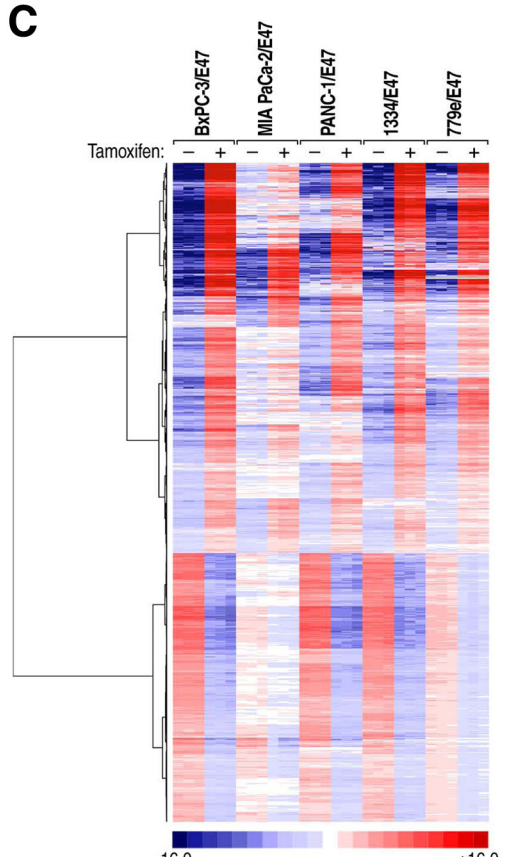
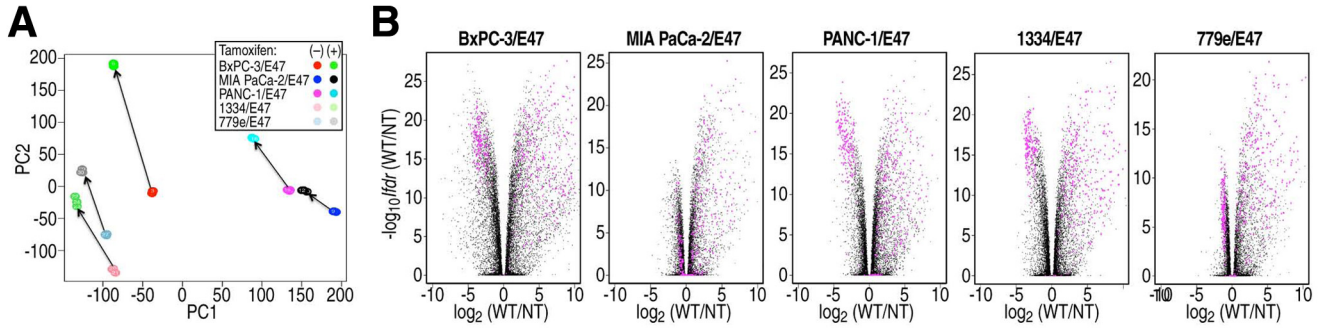
To begin mechanistic studies, we characterized 2 clinically relevant patient-derived cell lines that were recently generated from resected human PDA tumors. The cell line 779e was from a primary pancreatic tumor and cell line 1334 was from a PDA liver metastasis from a different patient.<sup>23</sup> Because PDA generally is diagnosed after metastasis, it was important to determine whether E47 also could induce growth arrest in 1334 cells.

Whole-exome sequencing identified the genetic status of KRAS, p53, p16, and SMAD4. KRAS G12V mutations, which disable guanosine triphosphatase activity and result in constitutive activation, were found in both 1334 and 779e cells (Figure 1A). Sanger sequencing validated the results and showed that the KRAS G12V mutation is mono-allelic in 1334 cells (Figure 1B). This mutation is comparable in oncogenic potential to the previously identified KRAS G12C and G12D mutations in MIA PaCa-2 and PANC-1 cells, respectively.<sup>24</sup> BxPC-3 was the only cell line in our study with a wild-type KRAS locus.<sup>24</sup> At the p53 locus, 1334 cells contained the most common cancer mutation, R175H, which causes structural distortions in the DNA binding domain.<sup>25</sup> In 779e cells, p53 harbored an R209K missense mutation and a single-nucleotide insertion in codon 210 that introduced a premature stop at codon 215 (Figure 1C). Using the monoclonal antibody DO-1, which is specific for the p53 N-terminus, the p53 protein was undetectable at any molecular weight in 779e cell extracts (Figure 1D and E). The CDKN2A/p16<sup>INK4A</sup> locus, which is deleted in the 3 ATCC cell lines, was present in both 1334 and 779e cells, but expressed only in 1334 cells (Figure 1A).<sup>24</sup> The SMAD4 locus, which is deleted in BxPC-3 cells, encoded wild-type protein that was expressed in the other 4 cell lines (Figure 1D).

### Induction of Nuclear E47 Caused Cell-Cycle Arrest in Primary Cell Lines

As performed previously for BxPC-3, MIA PaCa-2, and PANC-1, the 1334 and 779e cell lines were transduced with a retroviral vector expressing a form of E47 that translocated to the nucleus in response to tamoxifen (Figure 1F).<sup>22</sup> After 72 hours of tamoxifen treatment, the number of cells in all 5 E47-expressing cell lines was between 14% and 23% of control samples. Thus, E47 inhibited proliferation of primary cell lines as previously observed in established cell lines (Figure 1G).

Flow cytometry, used to assess DNA content after E47 induction, showed that the percentage of cells in G1 increased in all 5 lines (range, 9%–41%) whereas the percentage in S phase decreased (range, 18%–41%), suggesting that the cell cycle primarily was arrested before the G1/S transition. Interestingly, although the percentage of cells in G2/M increased 13% in 1334 cells and 6% in 779e cells, only MIA PaCa-2 among the established lines showed an increase, suggesting that primary cell lines may have retained active G2/M checkpoints (Figure 1H).



**D**

1334/E47			
Gene Symbol	Fold Change (WT/NT)	P value	RNA-seq lfr
AURKA	0.15	.003023	1.60E-19
AURKB	0.08	.000384	1.17E-14
BCL2	0.17	.000663	1.24E-08
BIRC5	0.1	.005944	1.80E-18
BRCA1	0.27	.000048	3.99E-15
BRCA2	0.15	.000942	5.42E-12
CCNA2	0.1	.0007	1.60E-22
CCNB1	0.12	.007303	4.83E-19
CCNB2	0.11	.000123	2.06E-19
CCND1	1.95	.046964	9.62E-06
CCDN2	434.54	.000585	1.54E-21
CCNE1	0.54	.021745	3.30E-10
CCNF	0.24	.000261	5.06E-18
ODC20	0.1	0	1.90E-19
CDC25A	0.21	.000351	3.81E-15
CDC25C	0.1	.001991	7.32E-19
CDC34	7.41	.000329	4.46E-11
CDC6	0.15	.000306	4.90E-21
CDK1	0.14	.000873	4.77E-19
CDK2	0.64	.034316	6.64E-13
CDK4	0.62	.014604	2.88E-12
CDK5R1	5.92	.006188	3.46E-15
CDK6	0.55	.004878	3.12E-07
CDKN1A	16.11	0	3.07E-18
CDKN3	0.19	.000229	1.66E-17
CHEK1	0.27	.020247	4.69E-20
CHEK2	0.38	.039966	2.61E-16
CKS1B	0.24	.000078	1.05E-18
CKS2	0.25	.000026	1.03E-17
CUL1	1.87	.009569	3.27E-02
E2F1	0.27	.000616	8.64E-16
GTSE1	0.09	.000601	3.64E-18
KNTC1	0.26	.003339	4.92E-16
MAD2L1	0.11	.000024	4.65E-21
MCM2	0.28	.022512	3.21E-18
MCM3	0.39	.012382	1.46E-17
MCM4	0.23	.015567	2.27E-19
MCM5	0.36	.000173	3.51E-16
MKI67	0.13	.000324	3.01E-17
RAD51	0.19	.000258	1.20E-15
RBL1	0.33	.005413	5.63E-18
SKP2	0.31	.002834	1.41E-14
STMN1	0.47	.04402	5.40E-12
TFDP1	0.28	.02043	1.68E-19
TFDP2	2.04	.045306	1.87E-06

779e/E47			
Gene Symbol	Fold Change (WT/NT)	P value	RNA-seq lfr
AURKB	0.38	.041823	8.32E-05
BIRC5	0.33	.003536	6.76E-07
BRCA1	0.4	.02019	1.40E-09
BRCA2	0.33	.011033	1.11E-04
CCNA2	0.46	.00711	1.25E-12
CCNB1	0.34	.030797	2.59E-08
CCNB2	0.47	.037132	1.10E-10
CCND2	87.02	.013669	5.59E-13
CDK5R1	2.35	.043517	9.28E-13
CDKN1A	9.85	.000424	6.78E-19
CKS1B	0.5	.012593	1.15E-09
KPNA2	0.21	.019485	6.59E-11
MAD2L1	0.52	.029116	6.33E-11
MCM2	0.46	.013032	1.92E-07
MKI67	0.44	.043377	1.54E-08
TFDP1	0.34	.029141	2.67E-10

**E**

Level	GO term	Description	Raw conditional P value	Conditional PFP
1	GO:000722	telomere maintenance via recombination	1.20E-12	5.82E-05
1	GO:0006268	DNA unwinding involved in DNA replication	2.96E-06	1.97E-03
1	GO:0006297	nucleotide-excision repair, DNA gap filling	2.96E-06	5.73E-03
1	GO:0007076	mitotic chromosome condensation	4.85E-06	2.58E-03
1	GO:0007080	mitotic metaphase plate congression	3.63E-06	2.20E-03
1	GO:0032467	positive regulation of cytokinesis	5.41E-06	2.74E-03
1	GO:0034080	CENP-A containing nucleosome assembly	2.54E-09	6.82E-05
1	GO:0034501	protein localization to kinetochore	2.15E-06	1.65E-03
1	GO:0060707	trophoblast giant cell differentiation	4.85E-06	2.58E-03
2	GO:0000022	mitotic spindle elongation	7.98E-05	9.16E-03
2	GO:0000083	regulation of transcription involved in G1/S transition of mitotic cell cycle	2.15E-07	3.72E-04
2	GO:0006270	DNA replication initiation	1.06E-15	6.18E-05
2	GO:0032355	response to estradiol	2.11E-06	1.18E-03
3	GO:0007052	mitotic spindle organization	2.89E-05	4.90E-03
3	GO:0008608	attachment of spindle microtubules to kinetochore	5.99E-07	7.22E-04
4	GO:000724	double-strand break repair via homologous recombination	3.91E-07	8.40E-04
4	GO:0006271	DNA strand elongation involved in DNA replication	5.51E-07	1.03E-03
4	GO:0007051	spindle organization	5.60E-05	9.28E-03
5	GO:0000079	regulation of cyclin-dependent protein serine/threonine kinase activity	1.41E-06	1.86E-03
5	GO:0000086	G2/M transition of mitotic cell cycle	3.46E-06	3.39E-03
5	GO:0007126	meiotic nuclear division	1.80E-05	8.63E-03
11	GO:0000070	mitotic sister chromatid segregation	3.86E-07	8.59E-05
12	GO:0000819	sister chromatid segregation	9.83E-05	4.52E-03
12	GO:0007067	mitotic nuclear division	1.83E-08	6.31E-06
14	GO:0007059	chromosome segregation	6.06E-06	4.51E-04

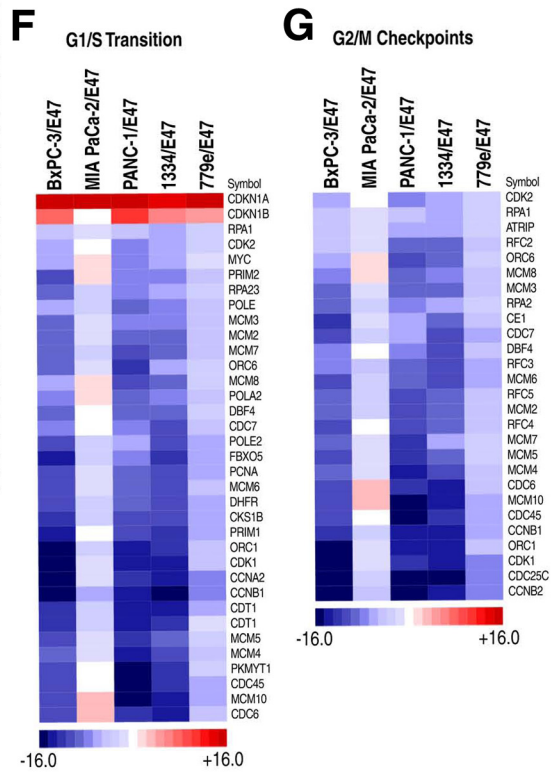


**Table 1. Antibodies Used**

Immunogen	Source	Supplier	Dilution
p53 ab-6 (clone DO-1)	Mouse	ThermoFisher (Waltham, MA)/ NeoMarkers (MS-187-P0)	Western blot 1:1000
p16	Rabbit	Abcam (Cambridge, MA) (ab81278)	Western blot 1:10,000
SMAD4	Rabbit	One World Lab (San Diego, CA) (ID 54398)	Western blot 1:3000
Vinculin	Rabbit	Cell Signaling Technology (Danvers, MA) (4650S)	Western blot 1:2000
p21	Mouse	Santa Cruz Biotech (Santa Cruz, CA) (sc-6246)	Western blot 1:50
P27	Rabbit	GeneTex (Irvine, CA) (GTX100446)	Western blot 1:2000/ICC 1:400
CEBP- $\alpha$	Rabbit	Abcam (ab40761)	Western blot 1:1000
Lamin B1	Rabbit	Abcam (ab16048)	Western blot 1:1000
CENP-A	Rabbit	Cell Signaling Technology (2186P)	Western blot 1:1000
RB pSER807/811	Rabbit	Cell Signaling Technology (8516S)	Western blot 1:2000
RB pSER608	Rabbit	Cell Signaling Technology (2181S)	Western blot 1:2000
RB	Mouse	Cell Signaling Technology (9309S)	Western blot 1:1000
GAPDH	Rabbit	Santa Cruz Biotech (sc-25778)	Western blot 1:1000
MYC	Mouse	DSHB (Iowa City, IA) (9E10-S, 32 $\mu$ g/mL)	Western blot 1:100
p53 pSER15	Rabbit	Abcam (ab1431)	Western blot 1:1000
p44/42 MAPK (ERK 1/2)	Rabbit	Cell Signaling Technology (4695T)	Western blot 1:1000
p44/42 MAPK (T202/Y204)	Rabbit	Cell Signaling Technology (4370T)	Western blot 1:2000
Ki67	Rabbit	Abcam (ab16667)	ICC 1:200
MYC (Y69)	Rabbit	Abcam (ab32072)	Western blot 1:1000
HA	Rabbit	Covance (Iowa City, IA) (PRB-101P HA.11)	Western blot 1:1000
pRSK	Rabbit	Abcam (ab32413)	Western blot 1:1000
RSK	Rabbit	Cell Signaling Technology (9333S)	Western blot 1:1000

### E47 Induced Global Transcriptomic Changes in All 5 Pancreatic Cancer Cell Lines

To gain insight into how E47 altered the transcriptome, genome-wide changes in gene expression that occurred after induction of E47 were characterized by RNA-seq. Total RNA isolated from triplicate control and tamoxifen-treated samples was used to generate 30 separate libraries that were multiplexed and subjected to paired-end 100 (100 base pairs) sequencing. Principal component analysis showed that all cell lines responded similarly to induction of E47 and that triplicate samples were highly consistent (Figure 2A). In each cell line, the data showed that a large fraction of genes underwent a statistically significant change in transcript levels ( $\text{lfdr} < 0.01$ ), with a wide range in magnitude, nominally up to 1000-fold (Figure 2B).

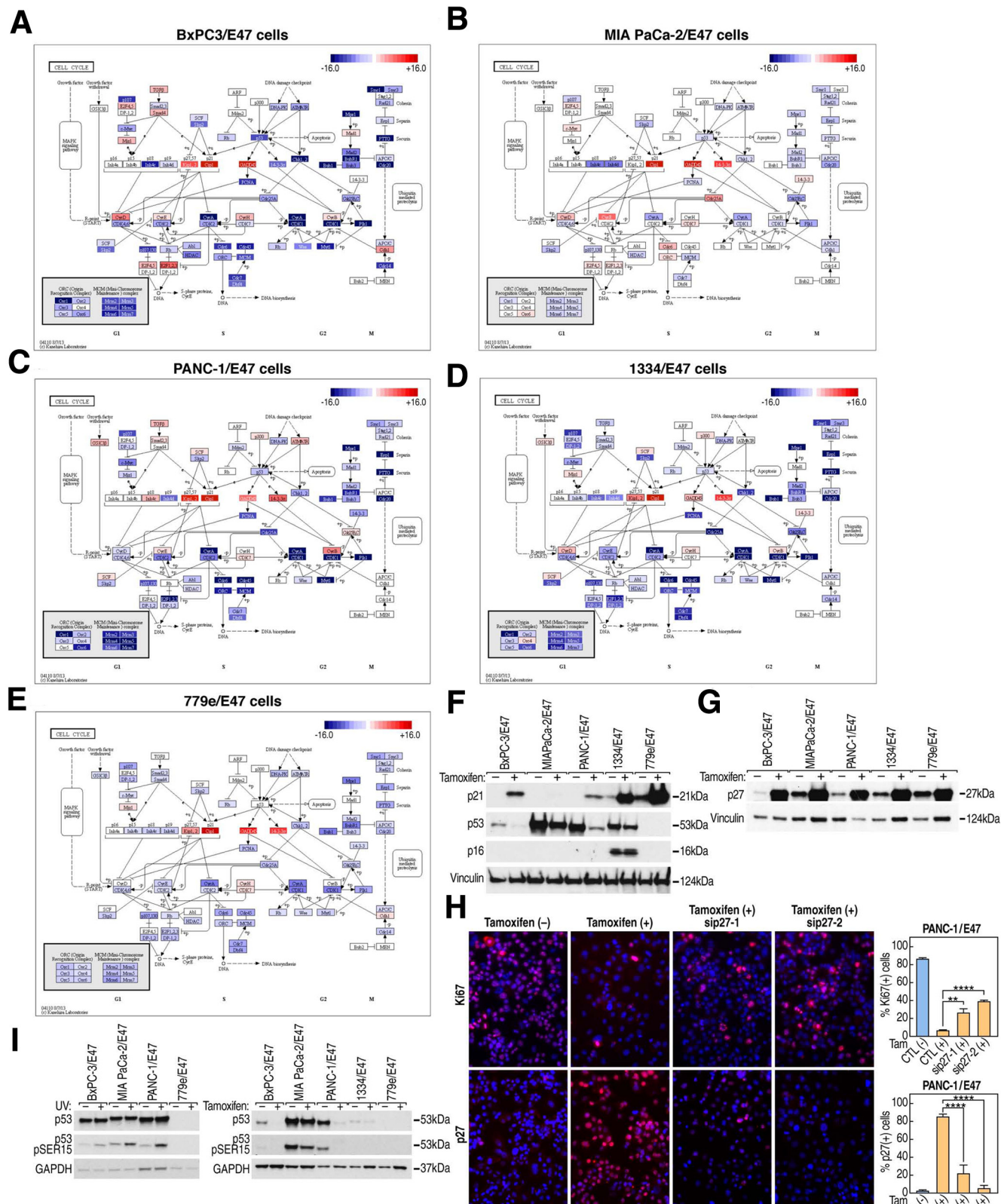
A series of statistical analyses identified genes that responded to E47 in a similar manner in all 5 cell lines (see the [Materials and Methods](#) section for derivation of  $s_5 > 100$ ). The 997 genes in this category had large and highly consistent changes in expression across all 5 cell lines. In a null model in which values were drawn randomly, the expected number of genes with  $s_5 > 100$  was approximately 39. Thus, the false discovery rate was approximately 39 of 977 (0.04), indicating high statistical significance. Genes with  $s_5 > 100$  were hierarchically clustered according to expression to show that transcript levels of approximately 60% were up-regulated and 40% were down-regulated (Figure 2C). Independent validation of changes in cell-cycle-associated genes identified by RNA-seq was performed using PCR array analysis (Figure 2D).

**Figure 2.** (See previous page). RNA-seq analysis showed that E47 systematically altered expression of a large cohort of cell-cycle control genes. (A) Principal component analysis identified highly consistent triplicates (overlapping circles) and similarity in response to induction of E47 (arrows) among the 5 cell lines. (B) Volcano plots of all genes (black and magenta dots) compared statistical significance ( $\text{lfdr}$ ) with magnitude of change in response to E47 ( $\log_2[\text{with tamoxifen (WT)/no tamoxifen (NT)}]$ ). Genes that showed a statistically significant change in transcript levels are represented by magenta dots. WT was to induce nuclear localization of E47, and NT is the control. (C) Hierarchical clustering of the 997 genes with the most statistically significant changes in transcript levels across all 5 cell lines as determined by RNA-seq ( $s_5 > 100$ , see the [Materials and Methods](#) section). (D) Changes in expression of some cell-cycle regulators initially identified by RNA-seq were validated using PCR arrays. (E) GO terms in the biologic process category derived from conditional GO analysis of the 997 genes with  $s_5 > 100$ . (F) Changes in transcript levels of all gene members of GO term regulation of transcription involved in G1/S transition of mitotic cell cycle. (G) Changes in transcript levels of all gene members of GO term G2/M check points.

**E47 Consistently Altered Expression of Cell-Cycle Control Genes**

Conditional GO analysis identified terms in the biological process category that were enriched for genes in the  $s_5$  >

100 data set.<sup>26,27</sup> Performed with a stringent threshold for statistical significance (posterior error probability, 0.01), this analysis identified 25 highly enriched biological processes (Figure 2E). Twenty-two of the GO terms were



related to cell division, showing a remarkably consistent response to E47 in the 5 cell lines.

Based on flow cytometry results (Figure 1E), we examined the expression of specific genes in the G1/S transition (Figure 2F) and G2/M checkpoint G0 terms (Figure 2G). Consistent with our previous findings, highly statistically significant increases in the CDK inhibitor, CDKN1A/p21<sup>CIP1</sup>, were noted.<sup>22</sup> Here, we observed that transcript levels of CDKN1B/p27<sup>KIP1</sup> also were increased in all but MIA PaCa-2/E47 cells (Figure 2F). In contrast, CDK2 and its activator, cyclinA2, which promote DNA replication in the S-phase through phosphorylation of prereplication complex subunits, were down-regulated<sup>28</sup> (Figure 2F). In addition, CDK1 and cyclinB1, which are required in G2 for chromosome condensation and nuclear envelope breakdown, were down-regulated (Figure 2G). Notably, the level of MYC transcripts also decreased in response to E47 in all but MIA PaCa-2 cells (Figure 2F).

### E47-Mediated Cell-Cycle Arrest Is CDKN1B/p27<sup>KIP1</sup>-Dependent

To provide an integrated picture of how E47 may have altered the biological interactions that control cell proliferation, we mapped changes in the transcript levels of all cell-cycle-associated genes in the RNA-seq data set onto the integrated Kyoto Encyclopedia of Genes and Genomes cell-cycle pathway (Figure 3A–E).<sup>29,30</sup> In accord with increased transcript levels, Western blot analysis showed increased CDKN1A/p21<sup>CIP1</sup> protein in 1334 and 779e cells, as previously reported in the ATCC lines (Figure 3F).<sup>22</sup> In addition to CDKN1A/p21<sup>CIP1</sup>, other traditional p53 targets, such as GADD45 and 14-3-3 $\sigma$ , also were up-regulated but perhaps not as a result of p53 activation given that 779e cells express no detectable p53 protein and that E47 repressed the expression of mutant p53 mRNA and protein in the other 4 lines (Figure 3A–F). Only 1334 cells express CDKN2A/p16<sup>INK4A</sup> transcripts and protein, neither of which changed in response to E47, indicating that altered CDKN2A/p16<sup>INK4A</sup> expression was not a mechanism used by E47 to block cell-cycle progression (Figure 3F).

After induction of E47, Western blot analysis and immunostaining showed a significant increase in CDKN1B/p27<sup>KIP1</sup> protein that paralleled changes in CDKN1B/p27<sup>KIP1</sup> transcript levels (Figure 3G and H). Before induction of E47, we observed low levels of CDKN1B/p27<sup>KIP1</sup> protein localized to the cytoplasm. In response to E47, CDKN1B/p27<sup>KIP1</sup> protein was highly up-regulated and localized to the nucleus (Figure 3H). To assay possible

function of CDKN1B/p27<sup>KIP1</sup> in E47-mediated cell-cycle arrest, 2 unique small interfering RNAs were used to knock-down CDKN1B/p27<sup>KIP1</sup> in PANC-1/E47 cells. After induction of E47, immunostaining with Ki67 antibody showed that depletion of CDKN1B/p27<sup>KIP1</sup> resulted in a significant increase in proliferating cells. Thus, E47 relied on CDKN1B/p27<sup>KIP1</sup> to inhibit cell-cycle progression (Figure 3H).

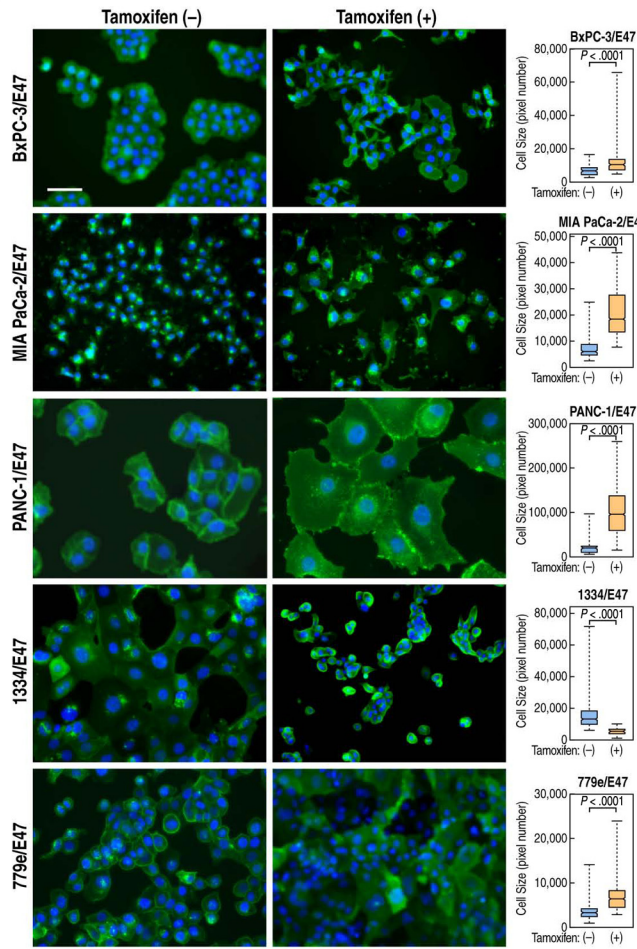
### E47-Mediated Cell-Cycle Arrest Is Associated With Biomarkers of Cellular Senescence

To determine whether E47 drives cells into a senescent state,<sup>31</sup> we used 2 widely accepted biomarkers of senescent cells: altered cell morphology and increased senescence-associated  $\beta$ -galactosidase (SA- $\beta$ gal) activity. In response to induction of E47, the cellular morphology of all 5 cell lines changed with all but 1334/E47 cells showing significantly increased cell size. In addition, a larger range of cell sizes was observed in all but 1334/E47 cells, indicating the presence of more diverse morphotypes as reported in senescent human fibroblasts<sup>32</sup> (Figure 4A). Assaying SA- $\beta$ gal activity at pH 6.0, which currently is regarded as one of the most reliable markers of senescence in PDA,<sup>33</sup> we observed a significant increase in all of the cell lines except BxPC-3/E47 after induction of E47 (Figure 4B). Of note, BxPC-3 is the only cell line of the 5 tested that lacks an oncogenic KRAS mutation.

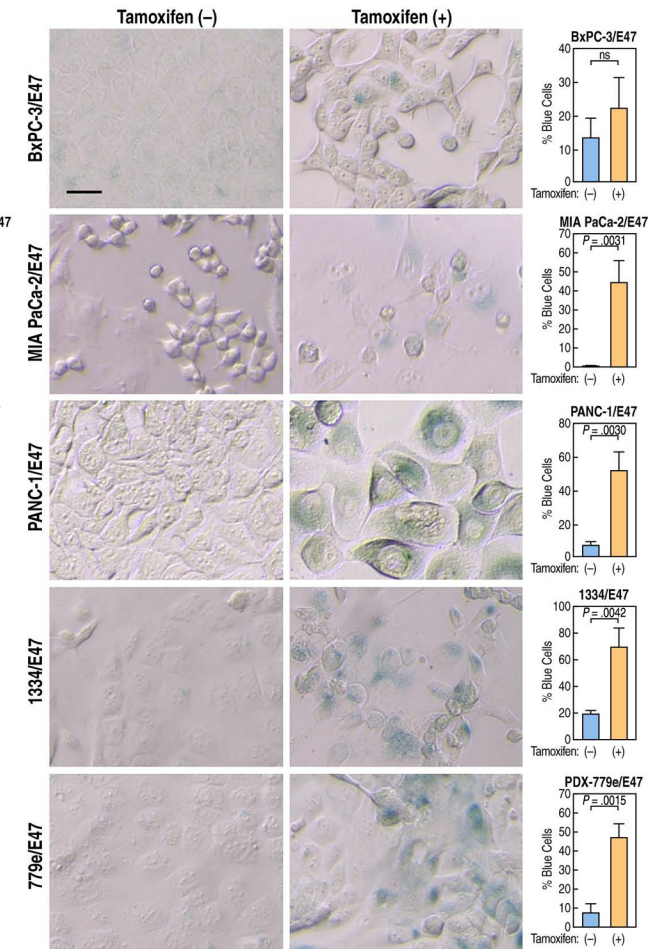
In addition to cytochemical changes, induction of E47 elicited a molecular signature of senescence in all 5 lines. Loss of Lamin B1, a nuclear membrane protein, is a biomarker of senescence that results from replicative exhaustion, oncogene expression, or DNA damage.<sup>34</sup> In response to E47, expression of Lamin B1 decreased at the RNA and protein levels in all 5 cell lines, suggesting possible involvement of p53 or RB signaling (Figure 4C).<sup>34</sup> We next asked if the ATM/ATR-mediated DNA damage response (DDR), as manifested by phosphorylation of SER15 in p53, might explain the decrease in Lamin B1.<sup>34</sup> Although  $\gamma$ -irradiation increased p53-SER15 in our cell lines, E47 induction did not, suggesting that E47-mediated senescence was independent of p53-mediated DDR (Figure 3J). CENP-A is an evolutionarily conserved centromere-specific histone H3 variant required for faithful segregation of chromosomes during cell division. In primary human fibroblasts, reduced expression of CENP-A induced cellular senescence.<sup>35</sup> In our experiments, induction of E47 led to lower expression of CENP-A protein in all but MIA PaCa-2 cells (Figure 4C). Conversely, CEBP- $\alpha$ , a tumor suppressor in multiple

**Figure 3.** (See previous page). In PDA cells, E47 directed an integrated program of gene expression that controlled cell cycle progression. (A–E) KEGG cell-cycle pathway reflecting E47-dependent alterations in expression of cell-cycle control genes in each cell line based on RNA-seq data. (F) Western blot analysis after induction of E47 showed increased CDKN1A/p21<sup>CIP1</sup> protein. (G) Western blot analysis after induction of E47 showed increased CDKN1B/p27<sup>KIP1</sup>. (H) shRNA knockdown of CDKN1B/p27<sup>KIP1</sup> in PANC-1/E47 cells resulted in an increased number of Ki67-positive cells after induction of nuclear E47. Data represent the mean of 6 separate fields, each with a minimum of 100 cells analyzed by an unpaired *t* test. Error bars are  $\pm$  SEM. (I) Left: Western blot analysis showed increased p53-pSER15 in response to  $2 \times 1610$  cGy of  $\gamma$ -irradiation (20 min of exposure on 2 consecutive days using a Gammacell40 Extractor, Research Irradiator with cesium 137 radiation source) to induce the DDR. Cells were harvested 3 hours after the second exposure. Right: Western blot analysis showed no increase in p53-pSER15 in response to induction of E47. \*\**P*  $\leq$  .01. \*\*\*\**P*  $\leq$  .0001.

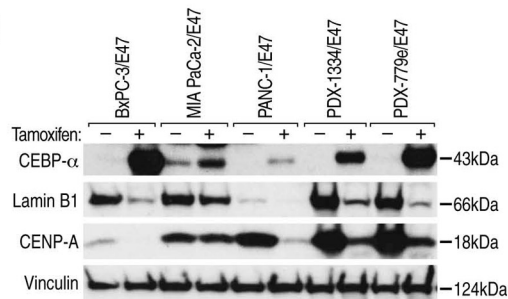
**A**



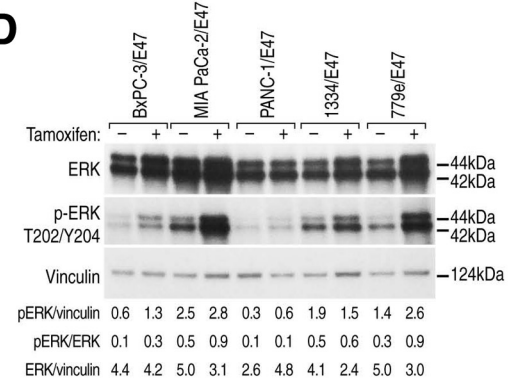
**B**



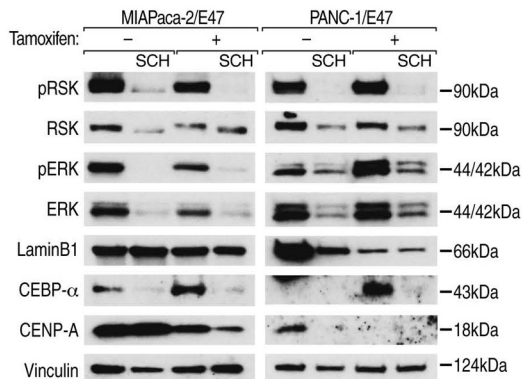
**C**



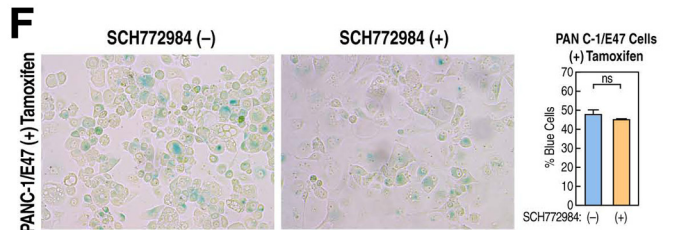
**D**



**E**



**F**



cancers, was up-regulated in response to E47. In PDA cells, decreased expression of CEBP- $\alpha$  was correlated with loss of KDM6B, a tumor suppressor that mediates oncogenic KRAS-induced senescence. The result was increased proliferation and aggressiveness of tumors.<sup>36,37</sup> Based on RNA-seq, E47 consistently up-regulated both KDM6B and CEBP- $\alpha$  transcript levels and we show that CEBP- $\alpha$  protein also was increased in all 5 cell lines (Figure 4C). Taken together, our data indicate that E47 induced both cytologic changes and a gene expression profile consistent with a cellular senescence phenotype in the absence of both CDKN2A/p16<sup>INK4A</sup> (except in 1334 cells) and wild-type p53.

Given the central role of oncogenic KRAS in PDA cell proliferation, we also considered that E47-induced growth arrest might occur through inhibition of KRAS activity. To address this possibility, we evaluated the T202/Y204 phosphorylation status of the KRAS effector, extracellular signal-regulated kinase (ERK). The data showed that the amount of phosphorylated ERK increased rather than decreased after E47 induction in all but 1334/E47 cells (Figure 4D). This paradoxical finding raised the possibility that by increasing KRAS signaling, E47 was stimulating an OIS response. To test this possibility, we treated MIA PaCa-2/E47 and PANC-1/E47 cells with the ERK inhibitor SCH772984<sup>13</sup> for 72 hours while simultaneously inducing E47. Western blot analysis of pRSK and phosphorylated ERK levels verified the activity of SCH772984 on the cells (Figure 4E). If activated ERK were required for senescence, we would have predicted that SCH772984 treatment would alter the expression of Lamin B1, CEBP- $\alpha$ , and CENP-A in a nonsenescent direction. The outcome, however, was that ERK inhibition altered expression of senescence markers in the prosenescent direction, thereby discounting activated ERK as the driver of senescence in response to E47 (Figure 4E). Furthermore, because OIS is an early response to mutant KRAS and is thought to require CDKN2A/p16<sup>INK4A</sup> and p53, this outcome supports the conclusion that E47 functions to block the cell cycle at points downstream of CDKN2A/p16<sup>INK4A</sup> and p53 signaling cascades. Finally, assay of SA- $\beta$ gal activity in PANC-1/E47 cells after induction of E47 was unaffected by treatment with SCH772984 (Figure 4F). We note that although SCH772984 did not alter E47-induced senescence, it did produce dramatic cell morphology changes

(ie, larger and flatter cells), in excess of what we observed with E47 alone.

### E47-Mediated Cell-Cycle Arrest is RB-Dependent

We next asked whether RB was required for E47-mediated cell-cycle arrest. One mechanism by which RB blocks cell-cycle progression involves direct interaction with E2F to repress transactivation of E2F target genes that control G1/S transition.<sup>38</sup> Consistent with this possibility, RNA-seq data showed that E47 decreased the expression of E2F target genes that regulate DNA replication in all lines except MIA PaCa-2/E47 (Figure 5A). Furthermore, as we observed in the G1/S transition GO term, E2F target genes that code for prereplication complex proteins (MCM2-7 and ORC1-6) and are required for licensing the G1/S transition, were also profoundly down-regulated (Figures 2F and 3A-F).

Because RB in its dephosphorylated state represses E2F target gene expression, we next examined how E47 affected RB phosphorylation status. Western blot analysis using antibodies specific for RB phospho-SER608 (pRB-608) and phospho-SER807/811 (pRB-807/811) showed significantly less phosphorylated RB after induction of E47 across all lines (Figure 5B). Total RB protein levels also were lower after E47 induction, as has been shown to occur in the G1 phase of the cell cycle (Figure 5B).<sup>39</sup>

To directly test the function of RB in E47-mediated cell-cycle arrest, BxPC-3/E47 cells were transduced with 2 unique short hairpin RNAs (shRNAs) against human RB. Expression of both shRB-1 and shRB-2 decreased the levels of RB protein (Figure 5C). An equal number of cells, transduced with either nonspecific shRNA, shRB-1, or shRB-2, were treated to induce E47, and immunostained with Ki67 antibody. The number of Ki67-positive cells was significantly higher after shRB knockdown (Figure 5D). To test if these results were due to off-target effects of the shRNAs, we transduced the shRB-1-infected cells with a second virus that expressed MSCV-driven hemagglutinin-tagged mouse Rb that would not be targeted by shRB-1. Western blot analysis showed expression of hemagglutinin-tagged mouse Rb that, unlike endogenous RB, persisted after induction of E47, presumably because

**Figure 4. (See previous page). E47 altered expression of cellular senescence biomarkers in a prosenescent direction.** (A) Cell size was measured after staining cell membrane glycoproteins with wheat germ agglutinin conjugated to Alexa 488. The median cell size was quantified based on pixel number, *P* values were determined by Mann-Whitney test, boxes represent the 2 middle quartiles, and whisker ends represent minimum and maximum data points. More than 50 cells were measured in each condition. (B) SA- $\beta$ gal activity was assayed at pH 6 after 72 hours of culture. For each condition in each cell line, data represent the mean of 3 separate fields, each with a minimum of 50 cells counted and compared by unpaired *t* test. Error bars are  $\pm$  SEM. Similar data were observed in 3 independent experiments. (C) Western blot analysis of CEBP- $\alpha$ , Lamin B1, and CENP-A after induction of E47. (B and C) Scale bars: 62.5  $\mu$ m; magnification, 200 $\times$ . (D) Western blot analysis of the effect of E47 induction on ERK expression and activation via phosphorylated ERK (pERK) T202/Y204. pERK and ERK signals were normalized to vinculin protein loading control. The ratio of pERK to ERK after normalization is shown. (E) Western blot analysis of whole-cell extracts from MIA PaCa-2/E47 and PANC-1/E47 cells after 72 hours of treatment with 5  $\mu$ m SCH772984 ERK inhibitor. (F) SA- $\beta$ gal activity assayed in PANC-1/E47 cells after 72 hours of E47 induction and simultaneous treatment with 5  $\mu$ m SCH772984. Data represent the mean of 6 separate fields, each with a minimum of 100 cells analyzed by unpaired *t* test. Error bars are  $\pm$  SEM.

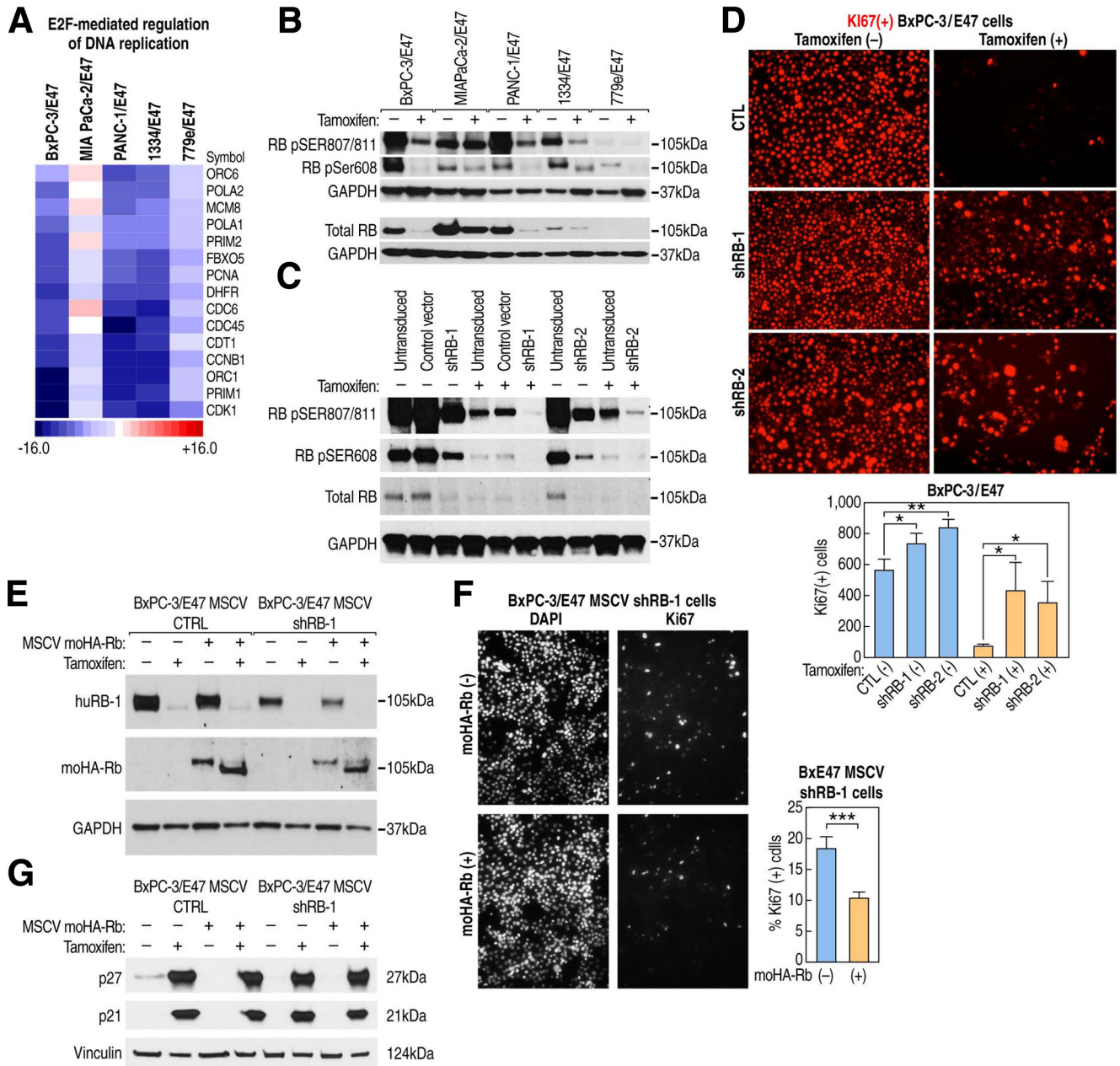


**Figure 5. RB is required for E47-mediated cell-cycle arrest.** (A) Transcripts encoding E2F target genes required for DNA replication are decreased. (B) Western blot analysis showed that phosphorylated RB (pSER807/811 and pSER608) decreased in response to E47. (C) Western blot analysis showing RB knockdown in BxPC-3/E47 cells. (D) BxPC-3 cells immunostained with Ki67 antibody after RB knockdown and induction of E47. Statistically significant increase in Ki67(+) cell numbers after knockdown of RB and induction of E47. Data represent the mean of 3 independent biological replicates analyzed by unpaired *t* test. Error bars are  $\pm$  SEM. (E) Western blot analysis of BxPC-3/E47 whole-cell extracts from cells harboring shRB-1 that targets the human RB gene (panel B) after transduction with a second virus expressing hemagglutinin-tagged mouse Rb under control of the MSCV promoter. (F) Immunostaining of the BxPC-3 cells expressing shRB-1 that targets human RB and  $\pm$  expression of MSCV-driven hemagglutinin-tagged mouse Rb after 72 hours of induction of E47. Cells were immunostained for Ki67 and counted. Data represent the mean of 6 separate fields, each with a minimum of 200 cells analyzed by unpaired *t* test. Error bars are  $\pm$  SEM. (G) Western blot analysis showing that expression of CDKN1B/p27<sup>KIP1</sup> and CDKN1A/p21<sup>CIP1</sup> is unchanged after rescue of Rb expression. \**P*  $\leq$  .05, \*\**P*  $\leq$  .01, \*\*\**P*  $\leq$  .001.

its expression was driven by the MSCV viral promoter and therefore not subjected to the same regulation as the endogenous RB gene (Figure 5E).<sup>40</sup> Interestingly, the majority of mouse Rb was a faster migrating species after E47 induction, potentially because of decreased

phosphorylation. After rescue with mouse Rb, cells again were again treated to induce E47 and immunostained with Ki67 antibody. We observed a statistically significant decrease in Ki67-positive cells, showing that RB is another required element of the E47-mediated program of

cell-cycle arrest (Figure 4F). In addition, we examined whether rescue of Rb expression in and of itself affected expression of CDKN1B/p27<sup>KIP1</sup> and CDKN1A/p21<sup>CIP1</sup> separate from induction by E47. Analysis by Western blot showed that expression of mouse Rb had no apparent effect on the level of CDKN1B/p27<sup>KIP1</sup> or CDKN1A/p21<sup>CIP1</sup> (Figure 5G).

### E47 Alters Proteosomal Degradation of MYC and CDKN1B/p27<sup>KIP1</sup>

RNA-seq analysis showed that MYC transcript levels decreased in all but MIA PaCa-2 cells in response to E47 (Figure 2F). Because MYC also is regulated critically via protein stability, we examined its expression by Western blot.<sup>41</sup> Strikingly, MYC protein levels significantly decreased in all 5 cell lines, including MIA PaCa-2, indicating that E47 can regulate MYC expression at multiple levels (Figure 6A).

We next asked whether E47 down-regulated MYC protein levels through proteosomal degradation. We compared the effect of 6-hour treatment with the proteasome inhibitor MG132 before and after induction of E47. In the 3 cell lines assayed (BxPC-3/E47, MIA PaCa-2/E47, and PANC-1/E47), we observed a modest but consistently higher level of proteosomal degradation after induction of E47 (Figure 6B). Therefore, decreasing transcript levels and/or promoting proteosomal degradation appeared to be 2 mechanisms by which E47 eliminated MYC expression. In the case of CDKN1B/p27<sup>KIP1</sup>, we observed the opposite effect. Here, proteosomal degradation slowed after induction of E47 (Figure 6B). In BxPC-3/E47 cells, induction of E47 also induced proteosomal degradation of mutant p53, but no effect was noted in MIA PaCa-2/E47 and PANC-1/E47 cells (Figure 6B). Regarding CDKN1A/p21<sup>CIP1</sup>, proteosomal control of protein levels occurred but was independent of E47 in all 3 lines consistent with E47 primarily controlling CDKN1A/p21<sup>CIP1</sup> expression at the RNA level (Figure 6B).

Because MYC is an E2F target gene, we asked whether RB knockdown affected MYC expression in BxPC-3/E47 cells and found that induction of E47 diminished MYC protein levels independent of RB expression (Figure 6C). Consistent with this, our treatment of BxPC-3/E47 cells with palbociclib (PD033291), a drug designed to specifically inhibit CDK4/6-dependent inactivation of RB, did not alter MYC, although it did slow PDA cell growth (Figure 6D).<sup>42</sup> Interestingly, PD033291 did not alter the effect of E47 on MYC in MIA PaCa-2/E47 and PANC-1/E47, but did lower MYC levels before induction of E47 in MIA PaCa-2/E47 and PANC-1/E47 cells (Figure 6D).

To test the function of MYC down-regulation in our system, we transduced PANC-1/E47 cells with lentiviruses expressing either wild-type or T58A mutant MYC, which prevents phosphorylation of THR58 typically leads to proteosomal degradation of MYC.<sup>41</sup> Western blot analysis of MYC protein levels in infected cells showed persistent expression of MYC even while inducing E47 (Figure 6E). The result of continued lentiviral expression of MYC while inducing E47 was a highly statistically significant increase in

the percentage of Ki67-positive cells, suggesting that down-regulation of MYC is another key component of the mechanism by which E47 blocks cell-cycle progression (Figure 6F).

## Discussion

In general, 2 classes of factors inhibit cell-cycle progression: members of the INK4 family and the CIP/KIP proteins CDKN1A/p21<sup>CIP1</sup> and CDKN1B/p27<sup>KIP1</sup>. INK4 proteins block the activity of CDK4/6 that monophosphorylates the RB tumor suppressor early in the G<sub>1</sub> phase of the cell cycle. Then, at the restriction point in late G<sub>1</sub>, CDK2, in complex with cyclin E, hyperphosphorylates RB, thereby releasing E2F transcription factors to drive expression of S-phase target genes.<sup>43</sup> CDKN1A/p21<sup>CIP1</sup> and CDKN1B/p27<sup>KIP1</sup> block the activity of CDK2 and CDK1 that control the G<sub>1</sub>/S and G<sub>2</sub>/M transitions, respectively. In pancreas cancer, the critical INK4 family member CDKN2A/p16<sup>INK4A</sup> often is silenced or deleted, CDKN1B/p27<sup>KIP1</sup> expression is lost and correlated with high tumor grade and advanced clinical stage,<sup>44</sup> and CDKN1A/p21<sup>CIP1</sup> is down-regulated in tumors from patients with shorter survival times.<sup>45,46</sup> Here, we report that induction of nuclear E47 up-regulates expression of CDKN1B/p27<sup>KIP1</sup>, rearms RB tumor-suppressor function, and down-regulates expression of MYC.

Previously, we showed that E47 increases CDKN1A/p21<sup>CIP1</sup> expression through direct binding to the promoter.<sup>22</sup> Other investigators have proposed that E47 binding to the CDKN1A/p21<sup>CIP1</sup> promoter enhances mRNA processing and/or stabilization, and is required for p53-dependent DDR induction of CDKN1A/p21<sup>CIP1</sup>.<sup>22,47</sup> In pancreatic cancer, the p53 gene often acquires mutations that may abrogate DNA binding and transactivation of CDKN1A/p21<sup>CIP1</sup>.<sup>48</sup> However, we show that E47 profoundly and independently up-regulates CDKN1A/p21<sup>CIP1</sup> mRNA and protein levels in the absence of DDR and in the background of 4 different p53 mutations, as well as in the complete absence of p53 protein.

The ability of CDKN1B/p27<sup>KIP1</sup> to halt the cell cycle by inhibiting the catalytic activity of CDK2 depends on the abundance, subcellular localization, and phosphorylation status of CDKN1B/p27<sup>KIP1</sup>, all of which can be regulated reciprocally by CDK2. Indeed, in a mouse model of PDA, haploinsufficiency of CDKN1B/p27<sup>KIP1</sup> accelerated PDA tumor development and shortened survival.<sup>49</sup> In our experiments, induction of E47 significantly increased steady-state levels of CDKN1B/p27<sup>KIP1</sup> transcripts and protein, and localized the protein to the nucleus. As in the case of CDKN1A/p21<sup>CIP1</sup>, there is evidence that CDKN1B/p27<sup>KIP1</sup> is a direct transcriptional target of E47.<sup>50</sup> In addition, transcription of CDKN1B/p27<sup>KIP1</sup> is activated by vitamin D receptor, which is among the most highly up-regulated genes in our RNA-seq data, and repressed by MYC, which is down-regulated significantly by E47.<sup>51,52</sup>

Proteolysis is also a key mechanism by which CDKN1B/p27<sup>KIP1</sup> levels are regulated. Interestingly, in all 5 PDA lines tested, RNA-seq showed a striking decrease in transcripts

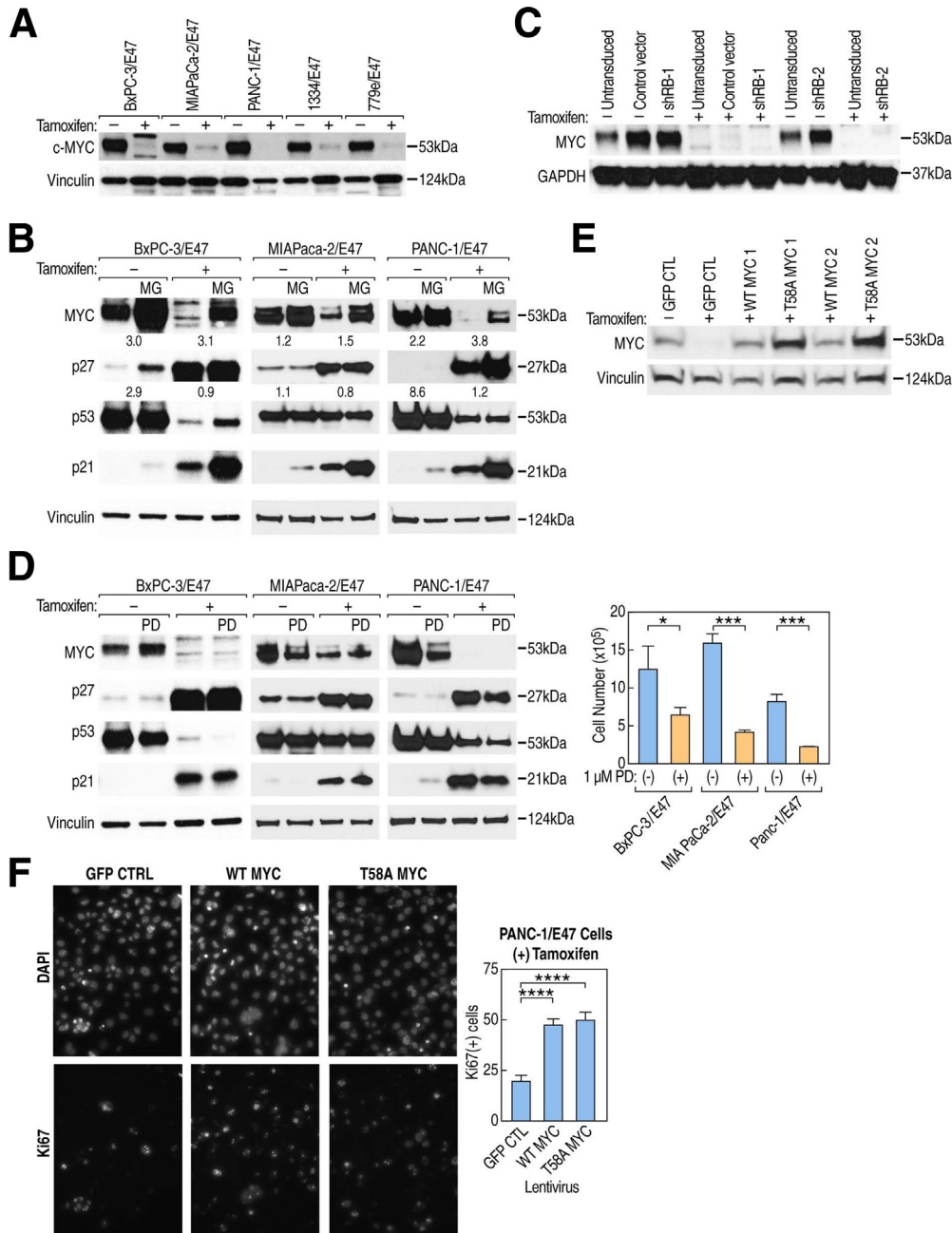


**Figure 6. E47 differentially regulates proteasomal degradation of MYC and CDKN1B/p27<sup>KIP1</sup>.** (A) MYC protein levels decrease after 72 hours of induction of E47 in all 5 cell lines. (B) Western blot of whole-cell extracts after 72 hours ± tamoxifen and 6 hours of treatment with 10 μmol/L MG132. The numbers below MYC and CDKN1B/p27<sup>KIP1</sup> represent the ratio of (+) MG132 to (-) MG132 after normalization of each band to the vinculin loading control. (C) shRNA RB knockdown in BxPC-3/E47 cells does not affect MYC expression when compared with the effect of control vector. (D) Western blot analysis of whole-cell extracts after 72 hours ± tamoxifen and 72 hours of treatment with 1 μmol/L PD033291. The effect of PD33291 on cell growth is reflected by the difference in cell number with treatment. Data were analyzed using an unpaired *t* test. Error bars are ± SEM of 3 independent biological replicates. (E) Western blot analysis of whole-cell extracts from PANC-1/E47 cells after transduction of lentivirus expressing either wild-type (WT) MYC or T58A degradation-resistant MYC. (F) PANC-1/E47 cells after transduction of lentivirus expressing either wild-type (WT) MYC or T58A MYC were treated with tamoxifen for 72 hours to induce E47. After treatment, cells were immunostained with Ki67 antibody and counted. The data represent the percentage of Ki67-positive cells. Six replicate wells, each with a minimum of 200 cells, were counted and analyzed by an unpaired *t* test. Error bars are ± SEM. \**P* ≤ .05, \*\*\**P* ≤ .001, \*\*\*\**P* ≤ .0001.

encoding 2 members of the SCF<sup>SKP2</sup> ubiquitin ligase complex: SKP2 and CKS1B. This may be significant because, after T187 phosphorylation of CDKN1B/p27<sup>KIP1</sup> by CDK2, CKS1B mediates interaction between CDKN1B/p27<sup>KIP1</sup> and SKP2, leading to proteosomal degradation of CDKN1B/p27<sup>KIP1</sup> in the nucleus.<sup>51,52</sup> Indeed, in a remarkable feat of drug development, small-molecule inhibitors that target a pocket formed at the protein–protein interface of SKP2 and CKS1 have been identified and shown to prevent polyubiquitylation and subsequent proteosomal degradation of CDKN1B/p27<sup>KIP1</sup> in cancer cells.<sup>53,54</sup> Regarding subcellular localization, CDK2 in complex with cyclin E can phosphorylate S10 in CDKN1B/p27<sup>KIP1</sup>, resulting in either CRM1-mediated nuclear export and proteolysis or further phosphorylation leading to assembly and nuclear localization of CDKN1B/p27<sup>KIP1</sup>/cycD/CDK4/6 complexes.<sup>51</sup> On balance, however, increased transcript levels and decreased degradation of CDKN1B/p27<sup>KIP1</sup> that result from induction of E47 combine to tip the balance in favor of stable nuclear CDKN1B/p27<sup>KIP1</sup>.

One of the most striking changes elicited by E47 was diminished expression of E2F S-phase target genes. This result suggested that E47 effectively blocked phosphorylation of RB, allowing it to inhibit E2F transactivation. This conclusion is supported by the observed decrease in levels of phosphorylated RB after induction of E47. The most likely explanation is that E47 enhanced CDKN1B/p27<sup>KIP1</sup> and CDKN1A/p21<sup>CIP1</sup>-mediated inhibition of CDK2 and CDK1, as described earlier, which reduced hyperphosphorylation and hence disarming of RB tumor-suppressor function.

That E47 might block cell-cycle progression by enhancing RB tumor-suppressor function is concordant with data from the *Kras*<sup>G12D</sup>; *Pdx1-cre* mouse model of PDA wherein deletion of RB in the background of the KRAS<sup>G12D</sup> mutation accelerated PDA and impaired senescence in premalignant lesions.<sup>55</sup> In the clinic, pharmacologic inhibitors of CDK4/6, such as palbociclib (PD033291), are being explored to block phosphorylation of RB in the treatment of PDA.<sup>56,57</sup> As we observed, palbociclib (PD033291) blocks PDA cell proliferation. It also increased oxidative phosphorylation in some lines, but induced epithelial-mesenchymal transition and enhanced cancer cell invasion in others.<sup>42,58</sup> Hence, specific blockade of CDK4/6 to rearm RB tumor-suppressor function may produce novel vulnerabilities but also elicit deleterious side effects, suggesting that reactivation of RB alone may be insufficient for long-term control of PDA cell growth.

Because MYC is a driver of PDA and opposes the actions of many E47-induced genes, MYC down-regulation is another critical component of E47-mediated cell-cycle arrest. At the RNA level, for instance, MYC represses transcription of the CDKN1A/p21<sup>CIP1</sup> and CDKN1B/p27<sup>KIP1</sup> genes whereas E47 increased CDKN1A/p21<sup>CIP1</sup> and p27 transcript levels.<sup>59,60</sup> In part, this may reflect competition for binding by MYC/MAX heterodimers, which also are bHLH proteins, to canonical E-box sequences (CACGTG), which are the preferred target sequences of E proteins such as E47.<sup>61</sup>

How E47 affects the steady-state levels of both MYC mRNA and protein remains an open question. As a primary

response gene, expression of MYC RNA is regulated by elongation from paused RNA polymerase II after recruitment of BET (bromodomain and extra terminal domain) and Mediator proteins.<sup>62</sup> These same proteins regulate superenhancers that control MYC expression in at least some cancers, but we found no evidence of altered RNA levels encoding these factors in our RNA-seq data.<sup>63</sup> We also did not find systematic alterations in other factors reported to control MYC transcription such as NFκB, β-catenin/TCF4, or NFATc1, which mediates transforming growth factor-β signaling.<sup>12</sup>

Although there is no evidence at this point that E47 directly regulates MYC transcription, E47 may indirectly down-regulate MYC RNA levels through rearming RB to repress E2F transactivation of target genes such as MYC. Arguing against this, however, are the data that shRNA knockdown of RB did not change MYC protein level (the effect on MYC RNA was not assessed) when compared with the effect of control vectors. At the protein level, there are conflicting reports on whether phosphorylation of MYC SER62 by KRAS-activated ERK or CDK2 stabilizes the protein or primes it for degradation.<sup>52</sup> E47 up-regulates ERK activity, which we might conclude primes MYC for degradation. However, inhibiting ERK does not block senescence—an outcome we would have predicted if ERK were responsible for MYC degradation. A more likely explanation is that by up-regulating CDKN1B/p27<sup>KIP1</sup>, E47 prevented stabilizing phosphorylation of SER62 by CDK2, which in turn might block senescence.<sup>64</sup> In either case, it is agreed that additional phosphorylation of MYC THR58 by GSK-3β followed by dephosphorylation of SER62 leads to SCF<sup>Fbw7</sup>-mediated proteosomal degradation. Interestingly, our RNA-seq data shows up-regulation of 2 genes that code for proteins involved in MYC degradation: *TRPC4AP* (Truss), which is an adaptor that mediates interaction between MYC and the DDB1-CUL4 E3 ligase, and *TRIM32*, which is an E3 ligase for MYC.<sup>41</sup>

In summary, our data offer new insight into how dysregulation of bHLH signaling may affect critical hallmarks of PDA including inhibition of RB and overexpression of MYC. We show that E47 reverses these pathogenic features and provokes a latent senescence response in PDA cells from primary tumors and metastatic lesions. To leverage these findings, we designed a screening platform to identify compounds that induce bHLH activity and used it to identify drugs of clinical relevance in PDA.<sup>65</sup> Together, our findings suggest that targeting E47 activity in PDA may be a novel and tractable approach to combat this recalcitrant cancer.

## References

1. Yachida S, Jones S, Bozic I, Antal T, Leary R, Fu B, Kamiyama M, Hruban RH, Eshleman JR, Nowak MA, Velculescu VE, Kinzler KW, Vogelstein B, Iacobuzio-Donahue CA. Distant metastasis occurs late during the genetic evolution of pancreatic cancer. *Nature* 2010; 467:1114–1117.
2. Bryant KL, Mancias JD, Kimmelman AC, Der CJ. KRAS: feeding pancreatic cancer proliferation. *Trends Biochem Sci* 2014;39:91–100.

3. De La OJ, Emerson LL, Goodman JL, Froebe SC, Illum BE, Curtis AB, Murtaugh LC. Notch and Kras reprogram pancreatic acinar cells to ductal intraepithelial neoplasia. *Proc Natl Acad Sci U S A* 2008; 105:18907–18912.
4. Habbe N, Shi G, Meguid RA, Fendrich V, Esni F, Chen H, Feldmann G, Stoffers DA, Konieczny SF, Leach SD, Maitra A. Spontaneous induction of murine pancreatic intraepithelial neoplasia (mPanIN) by acinar cell targeting of oncogenic Kras in adult mice. *Proc Natl Acad Sci U S A* 2008;105:18913–18918.
5. Kopp JL, von Figura G, Mayes E, Liu FF, Dubois CL, Morris JP, Pan FC, Akiyama H, Wright CV, Jensen K, Hebrok M, Sander M. Identification of Sox9-dependent acinar-to-ductal reprogramming as the principal mechanism for initiation of pancreatic ductal adenocarcinoma. *Cancer Cell* 2012;22:737–750.
6. Serrano M, Lin AW, McCurrach ME, Beach D, Lowe SW. Oncogenic ras provokes premature cell senescence associated with accumulation of p53 and p16INK4a. *Cell* 1997;88:593–602.
7. Campisi J, d'Adda di Fagagna F. Cellular senescence: when bad things happen to good cells. *Nat Rev Mol Cell Biol* 2007;8:729–740.
8. Guerra C, Collado M, Navas C, Schuhmacher AJ, Hernandez-Porrás I, Canamero M, Rodríguez-Justo M, Serrano M, Barbacid M. Pancreatitis-induced inflammation contributes to pancreatic cancer by inhibiting oncogene-induced senescence. *Cancer Cell* 2011; 19:728–739.
9. Jones S, Zhang X, Parsons DW, Lin JC, Leary RJ, Angenendt P, Mankoo P, Carter H, Kamiyama H, Jimeno A, Hong SM, Fu B, Lin MT, Calhoun ES, Kamiyama M, Walter K, Nikolskaya T, Nikolsky Y, Hartigan J, Smith DR, Hidalgo M, Leach SD, Klein AP, Jaffee EM, Goggins M, Maitra A, Iacobuzio-Donahue C, Eshleman JR, Kern SE, Hruban RH, Karchin R, Papadopoulos N, Parmigiani G, Vogelstein B, Velculescu VE, Kinzler KW. Core signaling pathways in human pancreatic cancers revealed by global genomic analyses. *Science* 2008;321:1801–1806.
10. Witkiewicz AK, McMillan EA, Balaji U, Baek G, Lin WC, Mansour J, Mollaei M, Wagner KU, Koduru P, Yopp A, Choti MA, Yeo CJ, McCue P, White MA, Knudsen ES. Whole-exome sequencing of pancreatic cancer defines genetic diversity and therapeutic targets. *Nat Commun* 2015;6:6744.
11. Zhu J, Sammons MA, Donahue G, Dou Z, Vedadi M, Getlik M, Baryte-Lovejoy D, Al-awar R, Katona BW, Shilatifard A, Huang J, Hua X, Arrowsmith CH, Berger SL. Gain-of-function p53 mutants co-opt chromatin pathways to drive cancer growth. *Nature* 2015;525:206–211.
12. Hessmann E, Schneider G, Ellenrieder V, Siveke JT. MYC in pancreatic cancer: novel mechanistic insights and their translation into therapeutic strategies. *Oncogene* 2016; 35:1609–1618.
13. Hayes TK, Neel NF, Hu C, Gautam P, Chenard M, Long B, Aziz M, Kassner M, Bryant KL, Pierobon M, Marayati R, Kher S, George SD, Xu M, Wang-Gillam A, Samatar AA, Maitra A, Wennerberg K, Petricoin EF, 3rd, Yin HH, Nelkin B, Cox AD, Yeh JJ, Der CJ. Long-term ERK inhibition in KRAS-mutant pancreatic cancer is associated with MYC degradation and senescence-like growth suppression. *Cancer Cell* 2016;29:75–89.
14. Lin WC, Rajbhandari N, Liu C, Sakamoto K, Zhang Q, Triplett AA, Batra SK, Opavsky R, Felsher DW, DiMaio DJ, Hollingsworth MA, Morris JPt, Hebrok M, Witkiewicz AK, Brody JR, Rui H, Wagner KU. Dormant cancer cells contribute to residual disease in a model of reversible pancreatic cancer. *Cancer Res* 2013; 73:1821–1830.
15. Shi G, Zhu L, Sun Y, Bettencourt R, Damsz B, Hruban RH, Konieczny SF. Loss of the acinar-restricted transcription factor Mist1 accelerates Kras-induced pancreatic intraepithelial neoplasia. *Gastroenterology* 2009;136:1368–1378.
16. Krah NM, De La OJ, Swift GH, Hoang CQ, Willet SG, Chen Pan F, Cash GM, Bronner MP, Wright CV, MacDonald RJ, Murtaugh LC. The acinar differentiation determinant PTF1A inhibits initiation of pancreatic ductal adenocarcinoma. *Elife* 2015;4:1–25.
17. Vincent A, Omura N, Hong SM, Jaffe A, Eshleman J, Goggins M. Genome-wide analysis of promoter methylation associated with gene expression profile in pancreatic adenocarcinoma. *Clin Cancer Res* 2011; 17:4341–4354.
18. Maruyama H, Kleeff J, Wildi S, Friess H, Buchler MW, Israel MA, Korc M. Id-1 and Id-2 are overexpressed in pancreatic cancer and in dysplastic lesions in chronic pancreatitis. *Am J Pathol* 1999;155:815–822.
19. Lee SH, Hao E, Kiselyuk A, Shapiro J, Shields DJ, Lowy A, Levine F, Itkin-Ansari P. The Id3/E47 axis mediates cell-cycle control in human pancreatic ducts and adenocarcinoma. *Mol Cancer Res* 2011;9:782–790.
20. Dufresne M, Clerc P, Dieng M, Edir A, Couvelard A, Delisle MB, Fourmy D, Gigoux V. Id3 modulates cellular localization of bHLH Ptf1-p48 protein. *Int J Cancer* 2011; 129:295–306.
21. Wang LH, Baker NE. E proteins and ID proteins: helix-loop-helix partners in development and disease. *Dev Cell* 2015;35:269–280.
22. Kim S, Lahmy R, Riha C, Yang C, Jakubison BL, van Niekerk J, Staub C, Wu Y, Gates K, Dong DS, Konieczny SF, Itkin-Ansari P. The basic helix-loop-helix transcription factor E47 reprograms human pancreatic cancer cells to a quiescent acinar state with reduced tumorigenic potential. *Pancreas* 2015;44:718–727.
23. Chakedis J, French R, Babicky M, Jaquish D, Mose E, Cheng P, Holman P, Howard H, Miyamoto J, Porrás P, Walterscheid Z, Schultz-Fademrecht C, Esdar C, Schadt O, Eickhoff J, Lowy AM. Characterization of RON protein isoforms in pancreatic cancer: implications for biology and therapeutics. *Oncotarget* 2016;7:45959–45975.
24. Deer EL, Gonzalez-Hernandez J, Coursen JD, Shea JE, Ngatia J, Scaife CL, Firpo MA, Mulvihill SJ. Phenotype and genotype of pancreatic cancer cell lines. *Pancreas* 2010;39:425–435.
25. Joerger AC, Fersht AR. Structure-function-rescue: the diverse nature of common p53 cancer mutants. *Oncogene* 2007;26:2226–2242.

26. Brazma A, Robinson A, Cameron G, Ashburner M. One-stop shop for microarray data. *Nature* 2000; 403:699–700.
27. Gene Ontology C. Gene Ontology Consortium: going forward. *Nucleic Acids Res* 2015;43:D1049–D1056.
28. Lim S, Kaldis P. Cdks, cyclins and CKIs: roles beyond cell cycle regulation. *Development* 2013;140:3079–3093.
29. Manyam G, Biredinc A, Baranova A. KPP: KEGG pathway painter. *BMC Syst Biol* 2015;9(Suppl 2):S3.
30. Kanehisa M, Goto S. KEGG: kyoto encyclopedia of genes and genomes. *Nucleic Acids Res* 2000;28:27–30.
31. Sharpless NE, Sherr CJ. Forging a signature of in vivo senescence. *Nat Rev Cancer* 2015;15:397–408.
32. Bayreuther K, Rodemann HP, Hommel R, Dittmann K, Albiez M, Francz PI. Human skin fibroblasts in vitro differentiate along a terminal cell lineage. *Proc Natl Acad Sci U S A* 1988;85:5112–5116.
33. Caldwell ME, DeNicola GM, Martins CP, Jacobetz MA, Maitra A, Hruban RH, Tuveson DA. Cellular features of senescence during the evolution of human and murine ductal pancreatic cancer. *Oncogene* 2012;31:1599–1608.
34. Freund A, Laberge RM, Demaria M, Campisi J. Lamin B1 loss is a senescence-associated biomarker. *Mol Biol Cell* 2012;23:2066–2075.
35. Maehara K, Takahashi K, Saitoh S. CENP-A reduction induces a p53-dependent cellular senescence response to protect cells from executing defective mitoses. *Mol Cell Biol* 2010;30:2090–2104.
36. Yamamoto K, Tateishi K, Kudo Y, Sato T, Yamamoto S, Miyabayashi K, Matsusaka K, Asaoka Y, Ijichi H, Hirata Y, Otsuka M, Nakai Y, Isayama H, Ikenoue T, Kurokawa M, Fukayama M, Kokudo N, Omata M, Koike K. Loss of histone demethylase KDM6B enhances aggressiveness of pancreatic cancer through downregulation of C/EBPalpha. *Carcinogenesis* 2014;35:2404–2414.
37. Kumagai T, Wakimoto N, Yin D, Gery S, Kawamata N, Takai N, Komatsu N, Chumakov A, Imai Y, Koeffler HP. Histone deacetylase inhibitor, suberoylanilide hydroxamic acid (Vorinostat, SAHA) profoundly inhibits the growth of human pancreatic cancer cells. *Int J Cancer* 2007;121:656–665.
38. Dick FA, Rubin SM. Molecular mechanisms underlying RB protein function. *Nat Rev Mol Cell Biol* 2013; 14:297–306.
39. Mihara K, Cao XR, Yen A, Chandler S, Driscoll B, Murphree AL, T'Ang A, Fung YK. Cell cycle-dependent regulation of phosphorylation of the human retinoblastoma gene product. *Science* 1989;246:1300–1303.
40. Burkhardt DL, Ngai LK, Roake CM, Viatour P, Thangavel C, Ho VM, Knudsen ES, Sage J. Regulation of RB transcription in vivo by RB family members. *Mol Cell Biol* 2010;30:1729–1745.
41. Farrell AS, Sears RC. MYC degradation. *Cold Spring Harb Perspect Med* 2014;4:1–16.
42. Liu F, Korc M. Cdk4/6 inhibition induces epithelial-mesenchymal transition and enhances invasiveness in pancreatic cancer cells. *Mol Cancer Ther* 2012; 11:2138–2148.
43. Narasimha AM, Kaulich M, Shapiro GS, Choi YJ, Sicinski P, Dowdy SF. Cyclin D activates the Rb tumor suppressor by mono-phosphorylation. *Elife* 2014;3:1–21.
44. Juuti A, Nordling S, Louhimo J, Lundin J, von Boguslawski K, Haglund C. Loss of p27 expression is associated with poor prognosis in stage I-II pancreatic cancer. *Oncology* 2003;65:371–377.
45. Dergham ST, Dugan MC, Joshi US, Chen YC, Du W, Smith DW, Arlauskas P, Crissman JD, Vaitkevicius VK, Sarkar FH. The clinical significance of p21(WAF1/CIP-1) and p53 expression in pancreatic adenocarcinoma. *Cancer* 1997;80:372–381.
46. Grabliauskaite K, Hehl AB, Seleznik GM, Saponara E, Schlesinger K, Zuellig RA, Dittmann A, Bain M, Reding T, Sonda S, Graf R. p21(WAF1) (Cip1) limits senescence and acinar-to-ductal metaplasia formation during pancreatitis. *J Pathol* 2015;235:502–514.
47. Andrysiak Z, Kim J, Tan AC, Espinosa JM. A genetic screen identifies TCF3/E2A and TRIAP1 as pathway-specific regulators of the cellular response to p53 activation. *Cell Rep* 2013;3:1346–1354.
48. Biegling KT, Mello SS, Attardi LD. Unravelling mechanisms of p53-mediated tumour suppression. *Nat Rev Cancer* 2014;14:359–370.
49. Diersch S, Wenzel P, Szameitat M, Eser P, Paul MC, Seidler B, Eser S, Messer M, Reichert M, Pagel P, Esposito I, Schmid RM, Saur D, Schneider G. Efemp1 and p27(Kip1) modulate responsiveness of pancreatic cancer cells towards a dual PI3K/mTOR inhibitor in pre-clinical models. *Oncotarget* 2013;4:277–288.
50. Trabosh VA, Divito KA, D Aquada B, Simbulan-Rosenthal CM, Rosenthal DS. Sequestration of E12/E47 and suppression of p27KIP1 play a role in Id2-induced proliferation and tumorigenesis. *Carcinogenesis* 2009; 30:1252–1259.
51. Chu IM, Hengst L, Slingerland JM. The Cdk inhibitor p27 in human cancer: prognostic potential and relevance to anticancer therapy. *Nat Rev Cancer* 2008;8:253–267.
52. Hydrbring P, Castell A, Larsson LG. MYC Modulation around the CDK2/p27/SKP2 axis. *Genes (Basel)* 2017; 8:1–32.
53. Wu L, Grigoryan AV, Li Y, Hao B, Pagano M, Cardozo TJ. Specific small molecule inhibitors of Skp2-mediated p27 degradation. *Chem Biol* 2012;19:1515–1524.
54. Rico-Bautista E, Wolf DA. Skipping cancer: small molecule inhibitors of SKP2-mediated p27 degradation. *Chem Biol* 2012;19:1497–1498.
55. Carriere C, Gore AJ, Norris AM, Gunn JR, Young AL, Longnecker DS, Korc M. Deletion of Rb accelerates pancreatic carcinogenesis by oncogenic Kras and impairs senescence in premalignant lesions. *Gastroenterology* 2011;141:1091–1101.
56. Fry DW, Harvey PJ, Keller PR, Elliott WL, Meade M, Trachet E, Albassam M, Zheng X, Leopold WR, Pryer NK, Toogood PL. Specific inhibition of cyclin-dependent kinase 4/6 by PD 0332991 and associated antitumor activity in human tumor xenografts. *Mol Cancer Ther* 2004; 3:1427–1438.

57. Sherr CJ, Beach D, Shapiro GI. Targeting CDK4 and CDK6: from discovery to therapy. *Cancer Discov* 2016; 6:353–367.
58. Franco J, Balaji U, Freinkman E, Witkiewicz AK, Knudsen ES. Metabolic reprogramming of pancreatic cancer mediated by CDK4/6 inhibition elicits unique vulnerabilities. *Cell Rep* 2016;14:979–990.
59. Bretones G, Delgado MD, Leon J. Myc and cell cycle control. *Biochim Biophys Acta* 2015;1849:506–516.
60. Abbas T, Dutta A. p21 in cancer: intricate networks and multiple activities. *Nat Rev Cancer* 2009;9:400–414.
61. Guccione E, Martinato F, Finocchiaro G, Luzi L, Tizzoni L, Dall' Olio V, Zardo G, Nervi C, Bernard L, Amati B. Myc-binding-site recognition in the human genome is determined by chromatin context. *Nat Cell Biol* 2006; 8:764–770.
62. Fowler T, Ghatak P, Price DH, Conaway R, Conaway J, Chiang CM, Bradner JE, Shilatifard A, Roy AL. Regulation of MYC expression and differential JQ1 sensitivity in cancer cells. *PLoS One* 2014;9:e87003.
63. Loven J, Hoke HA, Lin CY, Lau A, Orlando DA, Vakoc CR, Bradner JE, Lee TI, Young RA. Selective inhibition of tumor oncogenes by disruption of super-enhancers. *Cell* 2013;153:320–334.
64. Hydbring P, Bahram F, Su Y, Tronnorsjo S, Hogstrand K, von der Lehr N, Sharifi HR, Lilischkis R, Hein N, Wu S, Vervoorts J, Henriksson M, Grandien A, Luscher B, Larsson LG. Phosphorylation by Cdk2 is required for Myc to repress Ras-induced senescence in cotransformation. *Proc Natl Acad Sci U S A* 2010;107:58–63.
65. Villarino N, Signaevskaia L, van Niekerk J, Medal R, Kim H, Lahmy R, Scully K, Pinkerton A, Kim S, Lowy A, Itkin-Ansari P. A screen for inducers of bHLH activity identifies pitavastatin as a regulator of p21, Rb phosphorylation and E2F target gene expression in pancreatic cancer. *Oncotarget* 2017;8:53154–53167.

---

Received July 13, 2017. Accepted May 8, 2018.

#### Correspondence

Address correspondence to: Kathleen M. Scully, PhD, or Pamela Itkin-Ansari, PhD, Sanford Burnham Prebys Medical Discovery Institute, 10901 North Torrey Pines Road, La Jolla, California 92037. e-mail: [kscully@sbsdsccovery.org](mailto:kscully@sbsdsccovery.org) or [pitkin@sbsdsccovery.org](mailto:pitkin@sbsdsccovery.org); fax: (858) 795-5298.

#### Acknowledgments

The authors thank Kristen Jepsen, Mahdieh Khosroheidari, and Hiroko Matsui at the University of California San Diego Institute for Genomic Medicine Core for RNA sequencing. The shRB-2 vector was a gift from Scott Lowe (Memorial Sloan Kettering Cancer Center). MSCV mouse Rb was a gift from Steve Dowdy (University of California San Diego). Lentiviral MYC vectors were gifts from Yanxin Pei (Children's National Medical Center, Washington, DC). Viruses were produced by the Sanford Burnham Prebys Viral Vector Core.

#### Author contributions

Kathleen M. Scully was responsible for the study concept and design, acquisition of data, analysis and interpretation of data, drafting of the manuscript, and critical revision of the manuscript for important intellectual content; Reyhaneh Lahmy was responsible for the study concept and design, acquisition of data, and analysis and interpretation of data; Lia Signaevskaia was responsible for technical support; Roman Sasik was responsible for the acquisition of data, statistical analysis and interpretation of data, and critical revision of the manuscript for important intellectual content; Rachel Medal was responsible for the acquisition of data and analysis and interpretation of data; Heejung Kim was responsible for technical support; Randall French was responsible for the generation of key reagents; Brian James was responsible for the acquisition of data and analysis and interpretation of data; Yifan Wu was responsible for technical support; Andrew M. Lowy was responsible for critical revision of the manuscript for important intellectual content and obtained funding; and Pamela Itkin-Ansari was responsible for the study concept and design, analysis and interpretation of data, critical revision of the manuscript for important intellectual content, obtained funding, and study supervision.

#### Conflicts of interest

The authors disclose no conflicts.

#### Funding

Supported by The Falk Medical Trust (P.I.-A.); Ride The Point, the Kevin Tang Family Foundation, National Institutes of Health grant 5R01CA155620 (A.M.L.); the Center for Translational Research Institute grant UL1TR00144 (R.S.); and Sanford Burnham Prebys National Cancer Institute Cancer Center Support grant P30 CA030199 to the Sanford Burnham Prebys Viral Vector Core, which produced the viruses.